GAZ ANTEP UNIVERSITY GRADUATE SCHOOL OF NATURAL & APPLIED SCIENCES

EFFECTS OF NITROGEN INCORPORATION INTO GaInAs/GaAs GROWN ON (111) SUBSTRATES

M. Sc. THESIS
IN
ENGINEERING PHYSICS

BY
Mehmet KAYA
JULY 2006

July 2006 M. Sc. in Engineering Physics Mehmet KAYA

Effects of Nitrogen Incorporation into GaInAs/GaAs Grown on (111) Substrates

M. Sc. Thesis
in
Engineering Physics
University of Gaziantep

Supervisor
Prof.Dr. Be ire GÖNÜL

by
Mehmet KAYA
July 2006

T.C.
GAZ ANTEP UNIVERSITY
GRADUATE SCHOOL OF
NATURAL & APPLIED SCIENCES
ENGINEERING PHYSICS

Name of the thesis: Effects of Nitrogen Incorporation into GaInAs/GaAs Grown on (111) Substrates
Name of the student: Mehmet KAYA
Exam date: 20.07.2006

Approval of the Graduate School of Natural and Applied Sciences

Prof. Dr. Sadettin ÖZYAZICI
Director

I certify that this thesis satisfies all the requirements as a thesis for the degree of Master of Science.

Prof. Dr. Zihni ÖZTÜRK
Head of Department

This is to certify that we have read this thesis and that in our opinion it is fully adequate, in scope and quality, as a thesis for the degree of Master of Science.

Prof. Dr. Be ire GÖNÜL
Supervisor

Examining Committee Members Title and Name-surname	signature
Prof. Dr. Bülent GÖNÜL (Chairman)	_____
Prof. Dr. Be ire GÖNÜL	_____
Assoc. Prof. Dr. Hayriye TÜTÜNCÜLER	_____
Assoc. Prof. Dr. A. Necmeddin YAZICI	_____
Asst. Prof. Dr. Nuran DO RU	_____

Dedicated to my family

ABSTRACT

EFFECT OF NITROGEN INCORPORATION INTO GaInAs/GaAs GROWN ON (111) SUBSTRATES

KAYA Mehmet

M. Sc in Engineering Physics

Supervisor: Prof. Dr Be ire GÖNÜL

July 2006, 69 Pages

The aim of this thesis work is to examine the orientation dependence of the critical thickness and material properties of effective mass, band-edge shift and emission wavelength in GaInNAS QWs. This work also investigates the effect of the growth direction on confined state energies and their corresponding wavefunctions.

Keywords: nitrogen incorporation, critical thickness, grown on (111) orientation, quantum wells

ÖZET

(111) YÖNÜNDE BÜYÜTÜLMÜ GaInAs/GaAs S STEM NDE AZOT KATKILAMANIN ETK LER

KAYA Mehmet

Yüksek Lisans Tezi

Fizik Mühendisli i

Tez Danı manı: Prof. Dr. Be ire GÖNÜL

Temmuz 2006, 69 Sayfa

Bu tez çalı masının amacı GaInNAS kuvantum kuyuların malzeme özelliklerinden olan etkin kütle, bant-kenarı kayması ve yayılım dalga boyunun kristalin büyütülme yönüne olan ba ımlılı ının incelenmesidir. Bu çalı ma ayrıca kristalin büyütülme yönünün hapsolmu enerji seviyelerine ve bunlara kar ılık gelen dalga boylarına olan etkisini ara tırır.

Anahtar Kelimeler: azot katkılama, kıritik kalınlık, (111) yönünde büyütme, kuvantum kuyuları

ACKNOWLEDGEMENT

The author would like to express his thanks to his supervisor, Prof. Dr Be ire GÖNÜL, for many stimulated discussions, guidance, encouragement, and suggestions in the construction of this work.

His special thanks also go to his family

I would also like to thank to Dr. Murat ODUNCUO LU for his helpful discussions

CONTENTS

page

LIST OF FIGURES

LIST OF TABLES

CHAPTER 1

INTRODUCTION

Quantum well devices have been the objects of intensive research during the last two decades. Some of the devices have matured into commercially useful products and form part of modern electronic circuits. The seed of quantum well devices was planted when Esaki and Tsu [1] suggested in 1969 that a heterostructure consisting of alternating ultra thin layers of two semicunductors with difference in the band gaps should exhibit some novel useful properties. Experiments were done on the proposed heterostructure in 1974 with GaAs and AlGaAs. The mismatch in the lattice constant of GaAs and AlAs being only 0.12%. It is easy to grow layers of GaAs and mixed compounds of GaAs and AlAs on each other with crystalline perfection. Experiments were done with structures consisting of GaAs layers sandwiched of AlGaAs layers, which from potential-barrier layers as the band gap of AlGaAs is larger than that of GaAs.

The next important experiment demonstrated in 1979 is the formation of a two dimensional electron gas on the GaAs surface of a AlGaAs/GaAs heterojunction. In the next time, a transistor was realized by using a AlGaAs/GaAs heterostructure in 1980. In parallel with the development of a transistor, research was also being done for realizing a laser by using a quantum well structure, as some advantages were envisaged for such a laser. The density of states being stair-case-like, the concentration of carriers is large at the band edges in quantum wells. Whereas in bulk material the concentration is zero at the band edges. The density of carriers is also larger in quantum wells for the same injection current as the carriers are confined in a narrower region. These two conditions were expected to cause a lowering of the threshold current density in quantum well lasers. An additional expected advantage was the possibility of tuning the laser wavelength by controlling the well width. The quantized energy levels being related to the inverse square of the

well width. The energy difference between the lowest energy level in the conduction band and the highest energy level in the valence band is determined by the well width. A desired lasing wavelenght can, therefore, be realized by a suitable design of the well structure.

Semiconductor heterostructures are ideal quantum structures to explore various interesting physical phenomena and novel device applications. Electronic states of the quantum well can be engineered by changing the material combination, alloy composition, layer thickness, doping level, and even the substrate orientation.

Quantum well laser may be considered as the most succesful quantum well device. It is now extensively employed in optical communication systems, bar-code scanners, laser arrays and erasable optical discs. Short wavelenght QWL's (quantum well lasers) are also being developed currently, which have promise of increasing the storage capacity of data storage systems by an order of magnitude.

Today's high-speed lasers operating at the wavelengths $\lambda \approx 1.3$ μm and 1.55 μm are exclusively made of InP-based heterostructures. While GaInAsP/InP distributed feedback lasers are well-established light sources for long-haul 1.55-μm fibre backbone networks, they are too expensive to meet the demands of hundreds of millions of lasers that may be exploited in the future short-haul communication networks at 1.3 μm. Other shortcomings of GaInAsP/InP structures are low power capacity and poor heat conductivity, and inapplicability to vertical cavity surface-emitting lasers (VCSELs). Low output power (P)—and a low characteristic temperature coefficient (T)—are inherent physical properties of InP lasers, not significantly improvable by any band-gap engineering, and are primarily due to the existence of small bandgap discontinuities between GaInAsP and InP, which limit electron confinement in the quantum wells (QWs) at high injection levels or elevated temperatures. Another Achilles' heel of the InP-based materials is a small refractive index difference (Δn) between the adjacent layers of InP-based distributed Bragg reflectors (DBRs) used as mirrors to form the Fabry–Perot microcavity of a VCSEL. A wafer bonding technique, where the active region is made of InP-based QWs and

the DBRs of AlGaAs/GaAs with large Δn, has yielded good results [2] but may not be amenable to volume production of VCSELs.

Dilute nitrides have emerged from conventional III-V semiconductors such as GaAs or InP by the insertion of nitrogen (N) into the group V sub-lattice, which has profound influence on the electronic properties of these materials and allows widely extended band structure engineering. This is expected to lead to novel devices, e.g. for optical data transmission, solar cells, biophotonics or gas sensing, some of which are already making their way into the market. Unlike in all other cases, where a reduction in bandgap energy is achieved by inserting an element increases the lattice constant, nitrogen accomplishes this and at the same time reduces the lattice constant. Thus smaller bandgaps can be achieved and the unusual role of nitrogen in the lattice also allows a tailoring of band alignments. Both of these effects have opened up a new dimension of band engineering and the rapid progress in the field led to the demonstration of high quality 1.3 μm lasers on GaAs. This in turn will allow extending inexpensive data transmission through optical fibers from the present range of about 300 m to a distance of 10 to 20 km and at the same time increasing the data rate by about a factor of four. Thus it will enable metro-area datalinks, which are presently considered to be the bottleneck for large-scale optical communications.

For the first time, quantum wells (QWs) on GaAs substrates can provide long emission wavelenghts up to 1.3 μm by using GaInNAs alloys. Much attention is focused on these N-diluted materials because of the new applications they offer to GaAs technology.

Despite their promising applications and the first encouraging experimental results, very little is known about the physical properties of such alloys. For instance the difficulty of incorporating nitrogen into GaInAs while maintaining good optical quality has provoked much work to establish an understanding of the underlying factors determining the optical quality of GaInNAs, such as composition, growth and annealing conditions. It is still far from establishing an understanding of band structure and its dependence on composition. Fundamental electronic interactions

such as electron-electron and electron-phonon scattering, dependence of effective mass on composition, strain and orientation, quantum confinement effects, galvanometric properties, and mechanisms for light emission in these materials, are yet to be fully understood.

GaAs-based dilute nitrides, GaInAs(Sb), hold all the possibilities to reach light emission at 1.3 μm and beyond, with only one decisive point missing—an easy way to do it. Nevertheless, increasing evidence is being provided that GaInNAs(Sb) will be suitable for long-wavelength lasers [3]. Besides its cost-effectiveness and robustness compared to InP, it can be used to prepare monolithic VCSELs, which would be ideally suited for high-performance 1.3-μm transmission systems.

Mixed group-V nitride alloy semiconductors, for example, GaNP, GaNAs and GaInNAs, are novel semiconductor materials developed in the 1990s. They are very promising because they can be used to make devices with superior performance because of their uncommon physical properties, such as huge bandgap bowing. As a result, they have been applied in laser diodes [4-5], solar cells [6], and heterobipolar transistors [7]. Their uncommon physical properties are consequences of the extraordinary chemical characteristics of nitrogen compared to other III–V elements. However, these chemical characteristics, in turn, cause difficulty in alloying nitrogen to III–V crystals and, thus, in growing mixed group-V nitride alloy semiconductors. A strongly non-equilibrium growth method and a highly reactive nitrogen precursor are essential for the growth of mixed group-V nitride alloy semiconductors. Hence, no one succeeded in growing them until 1992. GaNP and GaNAs were grown for the first time by Baillargeon et al. [8] and Sato et al. [9], respectively. Both groups developed and used original and unique growth apparatus. To obtain mixed group-V nitride alloy semiconductors with excellent crystallinity, and to accelerate the research on these semiconductors and the development of devices used with these materials, more conventional growth methods and apparatus were required. At the beginning of the 1990s, the nitrogen radical cell that could be attached to a conventional molecular beam epitaxy (MBE) system had already been developed and widely used for the p-type doping of II–VI crystals [10]. Although the nitrogen concentrations for doping and alloying are very different, in 1994, Kondow et al. [4]

developed an MBE method in which nitrogen radicals are used as the nitrogen precursor to grow mixed group-V nitride alloy semiconductors. This method can grow mixed group-V nitride alloy semiconductors with excellent crystallinity, so it has been widely adapted.

The development of dilute-nitrides such as GaNAs and GaInNAs has become the focus of a considerable recent research activity because they exhibit potentially attractive properties for a range of devise applications including lasers [11-12], photodetectors [13], solar cells [14], and transistor [15]. The term dilute-nitride is used to reflect the low nitrogen (< 5 %) content, but the effect of substituting a relatively small fraction of the group V element arsenic by one of smaller ionic radius is to dramatically decrease the bandgap energy and decrease the lattice parameter. Larson et al. [11] first proposed the quaternary GaInNAs compound in which increasing indium fraction reduces the bandgap but also increases the lattice parameter. It is possible to balance the nitrogen and indium contents of GaInNAs to target a narrow bandgap material and lattice-parameter matching to substrate materials such as gallium arsenide.

The large lattice parameter difference between GaAs and GaN (20%) make the ternary GaNAs alloy scientifically interesting. Since GaAsN is generally grown on GaAs substrates, strain arising from the mismatch will have an enormous effect on any alloy epilayer properties. Neugebauer and Van de Walle [16] have estimated that the equilibrium solubility of nitrogen in GaAs is of the order of only 2%, majing it necessary to use nonequilibrium growth methods. Due to its large miscibility gap, GaAsN tends to phase separate when the nitrogen content becomes appreciable [17], however, nitrogen incorporation up to nearly 15% has been reported using a nitrogen plasma source combined with a relatively low growth temperature of 500 °C on a GaP substrate [18].

In the quaternary GaInNAs alloy a larger body of evidence is available regarding the luminescence from low nitrogen containing (< 1 %) quantum-well-based structures. However, in many cases the emission wavelength falls just below 1.3 μm at room temperature and below [19] and it has been noted that the addition of

higher nitrogen concentrations rapidly degrades the microstructure beyond any optical use. Some reports of higher nitrogen containing materials have been made, and in particular GaInNAs quantum dots with 4% nitrogen have been observed to give peak emission characteristics up to 1.5 μm [20].

Many works have been reported on the growth, characterization and processing of InGaAsN based devices on (100) substrates, but very few have been published on misoriented (111) GaAs substrates. Critical layer thickness (CLT) for InGaAs quantum wells (QWs) grown on (111) GaAs was reported to be higher than for (100) orientation [21–22]. This Critical layer thickness for the InGaAsN is still not fully known, but could open the possibility of reaching longer wavelengths using (111) substrates, growing wider and unrelaxed QWs with less nitrogen content, improving the optical quality. Wavelengths as long as 1.5 μm have been reported at low temperature for this kind of orientation [23].

Strained quantum wells grown in these orientations are piezoelectric, such that their optical transitions are red-shifted relatively to the (100) ones. The (111) strained layers also show higher critical thicknesses for strain relaxation compared to the (100) oriented ones. These two properties should therefore lead to GaInNAs QWs emitting at higher wavelengths than (100) QWs.

Chapter 2 presents the theoretical models used throughout this thesis. The theoretical models of interpolation technique for material parameters, strain theory, band anti-crossing model for band-gap calculations and electron effective mass are provided and the corresponding calculated results are presented. The necessary comments are also made to explain the basic physical properties of the system under investigation.

It has been shown that critical thickness and material parameters of effective mass, band-edge shift and emission wavelength are all orientation dependent. Chapter 3 investigates these orientation dependent parameters for dilude-nitride systems providing the necessary theoretical background. Related calculations are discussed in terms of the nitrogen-free counterparts. Chapter 4 investigates the effect

of growth direction on confined energy states and their corresponding wavefunctions. Finally, chapter 5 summarizes the conclusions that we have obtained from the present work.

CHAPTER 2

THE THEORETICAL MODELS

2.1. Introduction

This chapter presents the theoretical models and the necessary comments on the validity of these models used throughout this thesis. We also provide the calculations that we have done for the corresponding theoretical models and make comments on these calculated results for the systems under investigation.

2.2. Concept of Lattice-mismatch Strain.

In this section, we introduce the concept of lattice mismatch strain by means of discussing how strain is built into a semiconductor device during epitaxial growth. The limits of the incorporation of advantageous elastic strain before the material plastically deforms with the onset of irreversible defects and dislocations is briefly discussed.

2.2.1. Growth and Critical Thickness

To introduce the concept of strain in semiconductor heterostructures, the growth of a thin epilayer of semiconductor with lattice constant a_e on a thick substrate of lattice constant a_s is considered. For a sufficiently thin epilayer, all of the strain will be incorporated elastically in the layer, as shown in Fig.2.1. for both compressively-strained and tensile-strained layers. Thus, positively(negatively) mismatched layers give rise to compressive(tensile) elastic strain in the plane of the structure, perpendicular to the growth direction, and an associated tensile(compressive) strain in the growth direction. For the purposes of this thesis growth along the (001) direction is only considered.

As the thickness of the strained layer increases the energy stored in the structure also increases until a critical thickness[24] is reached at which pointh plastic relaxation occursand defects and dislocations will become prevalent. This has a detrimental effect on the performance of optoelectronic devices; the defect and dislocation areas act as non radiative recombination centres degrading the devices efficiency and decreasing theintended in -built strain.

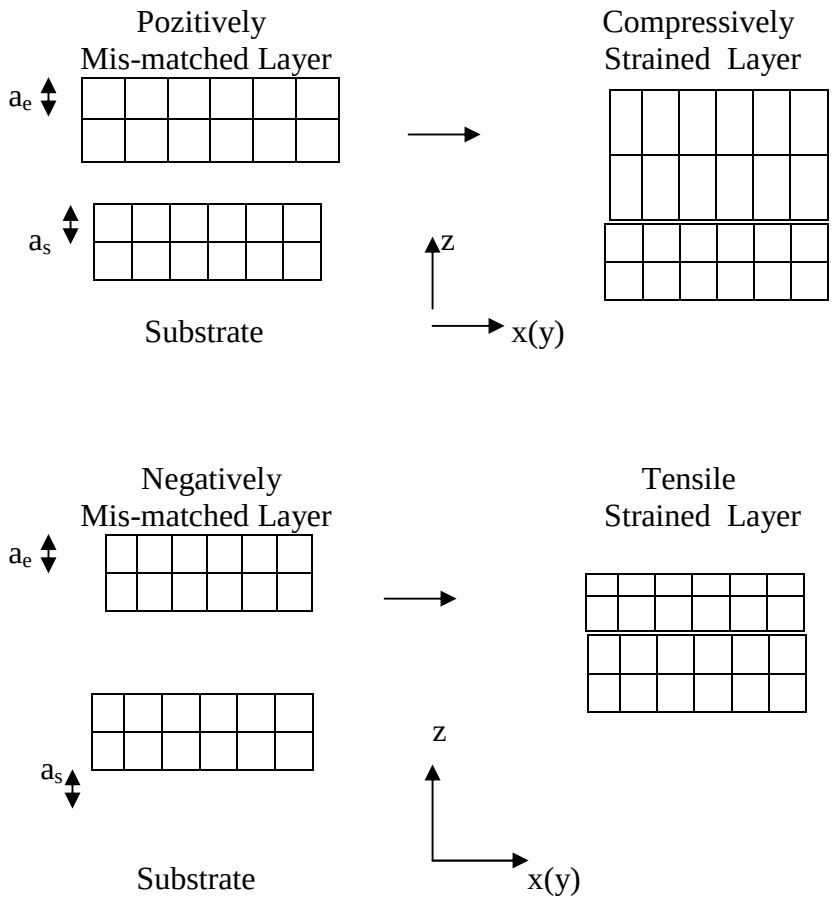

Figure 2.1 Schemtic diagram of growth of compressively-strained and tensile-strained layers grown on thick substrates.

Andersson[25] has demonstrated that high quality growth of $In_xGa_{1-x}As$ on GaAs can be achieved so long as the product of the lattice-mismatch strain and the later thickness is less than 200 % approximately. The critical thickness limit must be always be borne in mind when using strained laters in optoelectronic devices such as lasers.

2.2.2. Strain Theory

Consider the case of a compressively-strained layer. The epilayer is under a biaxial stress such that its in-plane lattice constant $a_{\|}$ equals the substrate lattice constant a_s. The net strain in the layer plane, $\epsilon_{\|,}$ is given by:

$$\varepsilon_{\|} = \varepsilon_{xx} = \varepsilon_{yy} = \frac{a_s - a_e}{a_e}$$

In response to the biaxial stress, the layer relaxes along the growth direction, the strain $\epsilon_{\perp}(=\epsilon_{zz})$ being of opposite sign to $\epsilon_{\|}$ and given by:

$$\varepsilon_{\perp} = -\frac{2\sigma}{1-\sigma}\varepsilon_{\|}$$

where σ is Poission's ratio. For tetrahedral semiconductors, σ is approximately 1/3 so that $\varepsilon_{\perp} \approx - \epsilon_{\|}$ [26]. The total strain can be resolved into a purely axial component, ϵ_{ax}, given by:

$$\epsilon_{ax} = \epsilon_{\perp} - \epsilon_{\|} \approx -2\epsilon_{\|}$$

and a hydrostatic component ϵ_{vol} (=ΔV/V), given by:

$$\epsilon_{vol} = \epsilon_{xx} + \epsilon_{yy} + \epsilon_{zz} \approx \epsilon_{\|}.$$

the resolution of the strain into components is important when modeling the effects of strain on the bandstructure of semiconductors and this will be dealt with more detail in the rest of the thesis.

2.3. Material Parameters and Calculations

The material parameters such as lattice constants and Luttinger parameters of the conventional ternary and quaternary systems can be calculated by linear interpolation method [27]. The material parameters depend on the well and barrier compositions, their widths and growth orientation. The parameters for the quaternary

alloy $Ga_{1-x}In_xN_yAs_{1-y}$ are interpolated from the binary compound values, such as B_{GaN}, B_{GaAs}, B_{InN}, and B_{InAs} using the following expression of [28]

$$Q_{GaInNAs}(x, y) = x\,y\,B_{InN} + x(1 - y)\,B_{InAs} + (1 - x)\,y\,B_{GaN} + (1 - x)(1 - y)\,B_{GaAs} \quad (2.1)$$

and the parameters for the ternary alloy $In_xGa_{1-x}As$ are interpolated from the binary compound values, such as B_{GaAs}, and B_{InAs} using the following expression of

$$Q_{InGaAs}(x) = x\,B_{InAs} + (1 - x)\,B_{GaAs} \quad (2.2)$$

where x is the fractional composition of indium, In, and y is the fractional composition of nitrogen, N, in GaInNAs [28]. The binary material values used in this thesis are given in Table 2.1.

Parameters	GaAs	InAs	GaN	InN
Lattice Constant a_o ($\mathring{A}$)	5.6533	6.0584	4.50	4.98
a_c(eV)	-7.17	-5.08	-6.71	- 2.65
a_v(eV)	-1.16	- 1.0	-0.69	- 0.7

Table 2.1 Binary material parameters [29].

Firstly we investigate the effect of the indium content of nitrogen free InGaAs/GaAs system. The lattice constant of the InGaAs increases with increasing indium content and band gap energy is decreasing with increasing indium content for both (001) and (111) growth orientation, as shown in Fig.2.2.

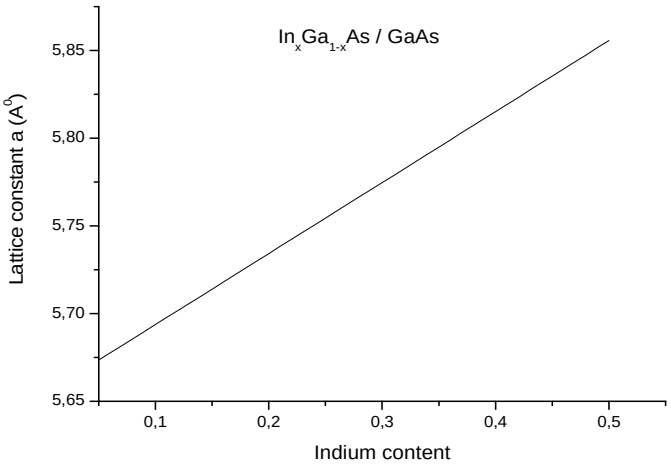

(a)

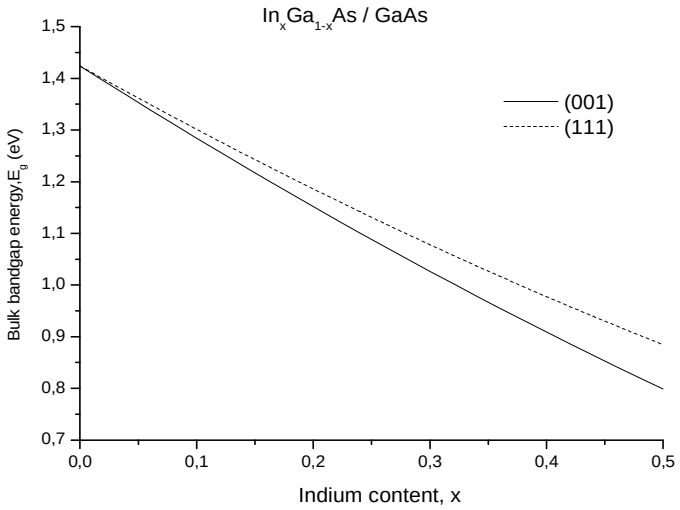

(b)

Figure 2.2 The variation of lattice constant (a) and band gap energy (b) with indium concentration in InGaAs.

The addition of indium into GaNAs to produce GaInNAs causes an increase in lattice parameters and a reduction in the bandgap [28] as shown in Fig.2.3. But the increase in nitrogen fraction in quaternary material of GaInNAs causes a decrease in lattice parameter and a reduction in the bandgap [28] which is shown in Fig.2.4. The change in lattice parameters for ternary and quaternary systems are calculated by using interpolation method.

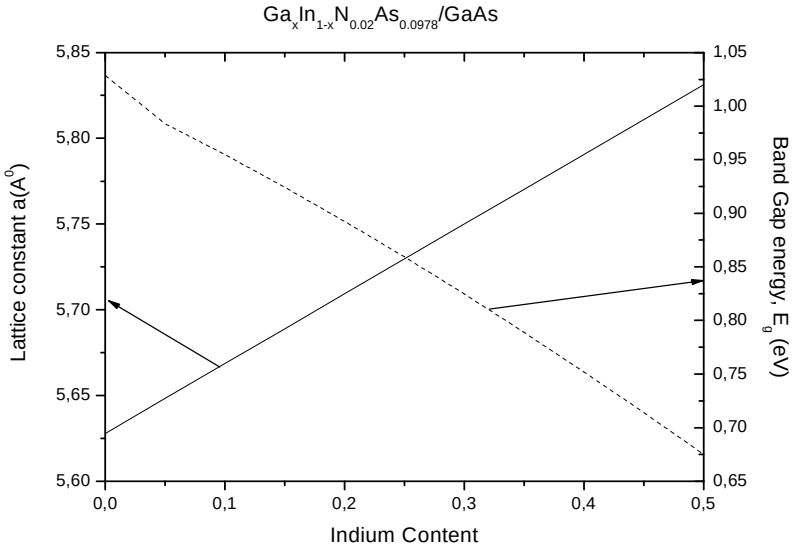

Figure 2.3 The variation of lattice constant and bandgap energy with indium concentration in GaInNAs.

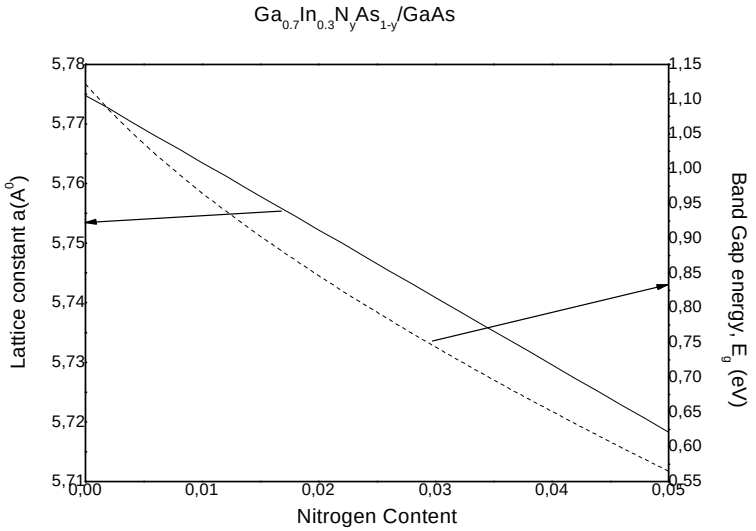

Figure 2.4 The variation of lattice constant and bandgap energy with nitrogen concentration in GaInNAs.

The change in lattice parameter and bandgap gives the flexibility of tailoring band structure. Hence, GaInNAs is a potential candidate to grow strained materials on GaAs substrate. Moreover, the effect of strain on the band structure varies with growth orientation. The lattice constant for any given composition of binary, ternary,

or quaternary well material compared with that of the substrate material determines whether the structure under investigation is unstrained laser device or not [28].

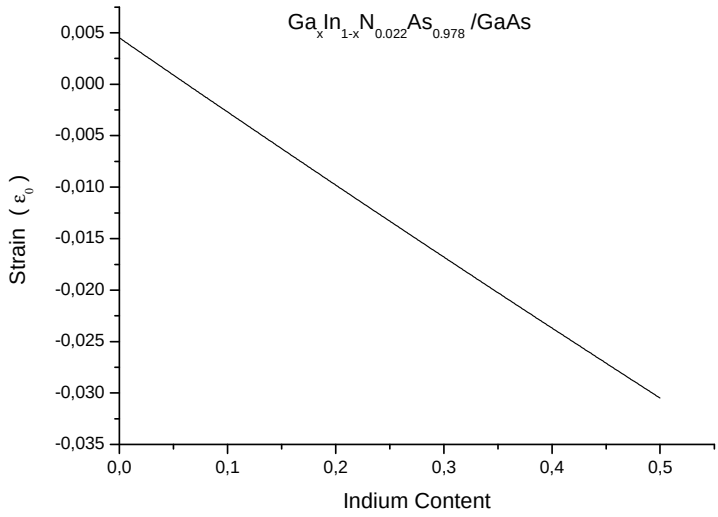

Figure 2.5 The variation of strain versus indium concentration in GaInNAs

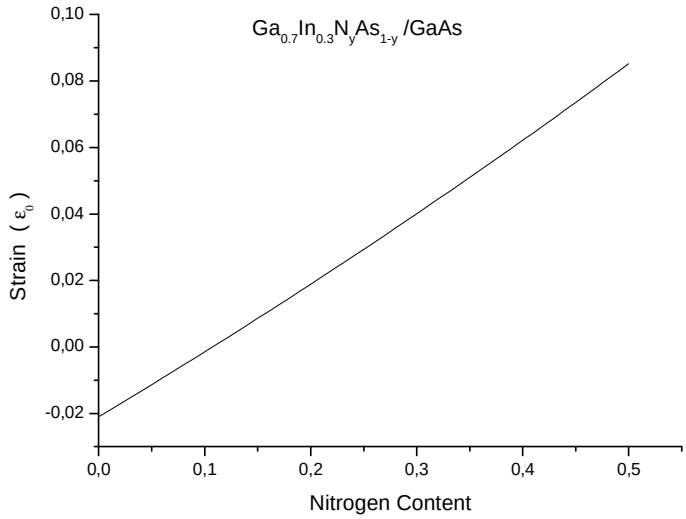

Figure 2.6 The variation of strain versus nitrogen concentration in GaInNAs

When the indium content in GaInNAs increases, strain decreases, on the other hand when the nitrogen content increases in GaInNAs, strain increases. Therefore,the effect strain is opposite in these two quaternary systems as shown clearly in Fig.2.5. and Fig.2.6.

2.4. The Band Anti-Crossing Model (BAC Model)

In recent years, $Ga_{1-x}In_xN_yAs_{1-y}$ has attracted considerable interest as a promising material for the realization of optoelectronic devices operating at telecom wavelengths in the near infrared. From a band structure point of view, the properties of this quaternary alloy are quite unusual [30]. We use the band anti-crossing model to explain this unusual system.

The bandgap energy has been successfully described for bulk semiconductor in terms of anti-crossing between the conduction band minimum of InGaAs and resonant band of localized nitrogen defect states above the band edge [31,32]. The two level band anti-crossing model (BAC) describes the electronic structure of $Ga_{1-x}In_xN_yAs_{1-y}$ [28]. In literature, some groups have been used this model and the results were found to be in good agreement [33-36].

According to band anti-crossing model, the incorporation of N into InGaAs (or GaAs) alloys leads to a strong interaction between the conduction band and a narrow resonant band formed by the N states. The overall effect is the splitting of the conduction band, with a consequent reduction of the fundamental bandgap due to the lowering of the conduction band edge [28]. The mathematical formalism of the model is derived as follows [34]. The interaction between the extended conduction states of the matrix semiconductor (InGaAs) and the localized N states is treated as a perturbation which leads to the following eigenvalue problem of [28]

$$\begin{vmatrix} E - E_M & -V_{MN} \\ -V_{MN} & E - E_N \end{vmatrix} = 0 \qquad (2.3)$$

where E_M is the conduction states of the matrix semiconductor, E_N is the localized nitrogen state energy (relative to the top of the valence band) and V_{MN} is the matrix element describing the interaction between these two states. Incorporation of the interaction represented by the matrix element V_{MN} leads to a mixing and anti-crossing of these states [28]. The solution to this eigenvalue problem gives us the dispersion relation for $Ga_{1-x}In_xN_yAs_{1-y}$ as

$$E_{\pm}(k) = \frac{E_M(k) + E_N + \sqrt{(E_M(k) - E_N)^2 + 4C_{MN}^2}}{2} \qquad (2.4)$$

The BAC model provides simple analytic expressions for the conduction band dispersion as a function of N concentration y and allows to calculate, for example, the strength of the optical transitions [37] in bulk materials and the transition energies between electronic states in quantum wells or the gain in laser structures [38].

A schematic diagram of the band structure for $Ga_{1-x}In_xN_yAs_{1-y}$ according to Eqn. (2.3), and the $E_{\pm}(k)$ and E_N levels, is calculated and shown in Fig. 2.7. All energies are measured relative to top of the valence band in this figure. The E_+ transition is blue shifted and the E_- transition is red shifted from the N resonant level with increasing N concentration. According to this model, the E_- subband has mainly delocalized conduction band-like character, whereas the E_+ subband is due to the localized E_N-like states. An increase in the V_{MN} value with increasing N concentration leads to a stronger repulsion between the E_- and E_+ states [28].

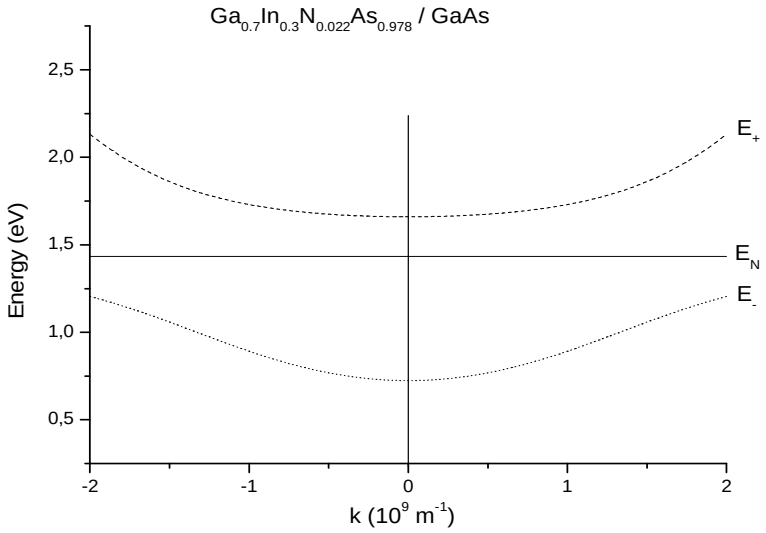

Figure 2.7 The calculated conduction band structure of $Ga_{0.7}In_{0.3}N_{0.022}As_{0.978}$ near the Γ-point (k = 0) according to the BAC model. A parabolic approximation for the conduction band of InGaAs was used. The splitting of the conduction band into E_- and E_+ bands is clearly shown. The energy scale is relative to the top of the valence band.

One of the most striking features of the results is a distinct flattening of the $E_{\pm}$ curves for energies approaching E_N. This indicates a large increase in the effective mass in both subbands compared to GaAs. A strong non-parabolicity of the conduction band can also be predicted from Fig. 2.7. The electron effective mass is another important material parameter and depend very strongly on the electron energy relative to localized E_N level [28].

2.5. Verification of the Band Anti-Crossing Model

In the literature it seems, so far, that the BAC model is well established as far as the macroscopic behavior is concerned. Shan et al. [34-36] measured optical transitions under pressure, where optical transitions are observed, which are associated with the two branches of the split lowest conduction band in GaInNAs for various compositions.

Skierbiszewski et al. [39] examined the carrier dynamics in a GaNAs alloy where they measured the mobility of carriers in the alloy and compared it to the theoretical mobility, calculated, from the BAC model; the qualitative and quantitative agreement of theory and experiment was good. These authors also examined the increase of the conduction band effective mass theoretically (in the context of the BAC model) and experimentally; again the agreement was very good [33].

Uesugi et al. [40] have indirectly confirmed the central idea of the model (i.e. the interaction of the extended and localized levels) through the temperature dependence of bandgap energies of GaNAs films for various N concentrations. The result showed that, in determining the temperature dependence of the bandgap energy, two kinds of N - related energy states with different temperature dependence of bandgap energy must be considered: one with a higher temperature dependence similar to the GaAs bands (extended like state) and an N-related localized state with lower temperature dependence [28].

Finally, Lindsay and O'Reilly [41] have adopted a theoretical approach. By using a tight-binding sp^3s^* Hamiltonian, they have calculated the compositional dependence of the conduction band edge and then compared it with the E_ energy calculated according to the BAC model. These results were found to be in good agreement, as well [28].

2.6. Parameters within the Band Anti-Crosssing Model

In order for the dispersion relation predicted by the model to reproduce the band structure of the real semiconductor as accurately as possible, the interaction matrix element V_{MN} and the nitrogen level E_M must be determined along with their dependence on composition. In addition, an accurate form for the electron effective mass is required for the calculation of various laser parameters [28]. The E_M is the energy of the InGaAs matrix conduction band and is given as [42],

$$E_M(k) = \begin{Bmatrix} E_0 - 1.55y + \dfrac{\eta^2 k^2}{2m}, & eV\ inside\ the\ well \\ E_0, & outside\ the\ well \end{Bmatrix} \tag{2.5}$$

where y denotes the nitrogen concentration and $\frac{\eta^2 k^2}{2m}$ is quadratic conduction band dispersion term, E_0 is the conduction band edge of the well/barrier material in the absence of nitrogen. The energy of the nitrogen level is taken as

$$E_N = \begin{Bmatrix} 1.52 - \gamma y, & eV\ inside\ the\ well \\ 1.52 + E_{b,N,} & outside\ the\ well \end{Bmatrix} \tag{2.6}$$

where $\gamma = 2.52$ for GaNAs and $\gamma = 3.9$ for GaInNAs. The height of the nitrogen barrier, $E_{b,N}$ and E_N are assumed independent of k and all the energies are taken relative to the top of the valance band. The strength of the $\Gamma - E_N$ interaction is described by the interband matrix element V_{MN} [28]. The square of the matrix element V_{MN}^2 is proportional to concentration of nitrogen atom as

$$V_{MN} = \begin{Bmatrix} C_{MN}\sqrt{y}, & inside\,the\,well \\ 0, & elsewhere \end{Bmatrix} \quad (2.7)$$

The V_{MN} is a key parameter describing the interaction between the localized and extended states. The values of V_{MN} is not constant and may be composition dependent [34-39]. In this thesis we have used the value of V_{MN} as $2.7\sqrt{y}$ eV [42].

Using these parameters we calculate these subband energies of E_- and E_+ versus nitrogen concentration as shown in Fig. 2.8. With increasing nitrogen concentration E_- energy shifts towards lower energies. On the contrary, the E_+ energy shifts towards higher energies with increasing nitrogen. The E_+ level has been found to increase linearly with a slope nearly equal to the decrease in E_- [28].

2.7. Electron Effective Mass

A knowledge of the carrier mass is necessary for analysis of important semiconductor properties. As is well known, the carrier mobility is strongly dependent upon the effective mass. In addition, the knowledge of the effect of the effective mass on gain parameters is of special importance for a full exploration and optimization of III-N-V material system in device applications. Therefore, the change in electron effective mass due to the nitrogen modified conduction band is investigated in this section [28].

Unlike other conventional alloy semiconductors, the electron effective mass increases when the energy bandgap is reduced by adding nitrogen [28]. This has a profound influence on the strength of electron-photon and electron-electron interactions, and consequently on every aspect of the performance (threshold current, etc.) of semiconductor lasers. We have calculated the subband energies of E_- and E_+ for $Ga_{0.7}In_{0.3}N_yAs_{1-y}$/GaAs and shown in Fig.2.8. As can be seen from this figure the energy E_- is flattening near its minimum leading to a large enhancement of the electron effective mass [28].

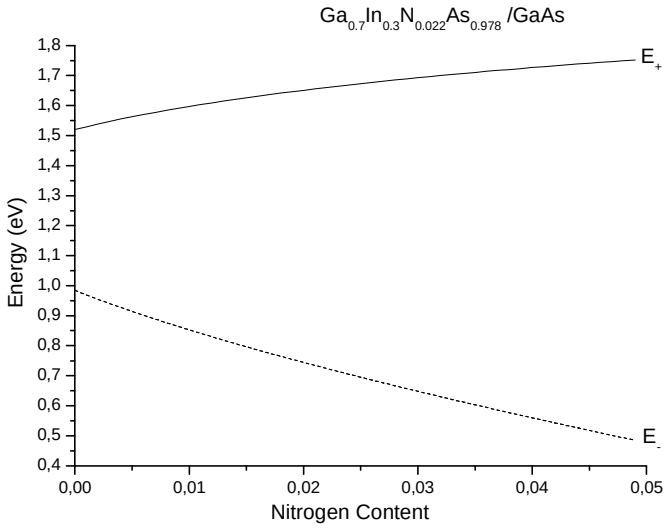

Figure 2.8 Calculated subband energies E_- and E_+ as a function nitrogen concentration for $Ga_{0.7}In_{0.3}N_yAs_{1-y}$, according to BAC model.

The change in electron effective mass due to the nitrogen modified conduction band can be found by Skierbiszewski et al. [39] as

$$m^* = m_M \left[1 + \left(\frac{V_{MN}}{\left(E_N - E_- \right)} \right)^2 \right] \tag{2.7}$$

where m_M is the electron effective mass in the parabolic conduction of the semiconductor matrix, m_M is calculated by following equation

$$m_M = x\, m_{M\,(InAs)} + (1-x)\, m_{M\,(GaAs)} \tag{2.8}$$

where $m_{M\,(InAs)}$ and $m_{M\,(GaAs)}$ values are given in Table 2.2.

Mass	GaAs	InAs
m_M (m_o)	0.067	0.026

Table 2.2 Binary material parameters [29].

We have calculated the change in electron effective mass due to the nitrogen-modified conduction band using the dispersion relation of Eqn.2.7. The electron effective mass of electron increases with nitrogen composition, as shown in Fig. 2.9. This behavior is rather unusual and in fact is opposite to the conventional semiconductors, where the value of effective mass decreases with decrease of bandgap energy [28].

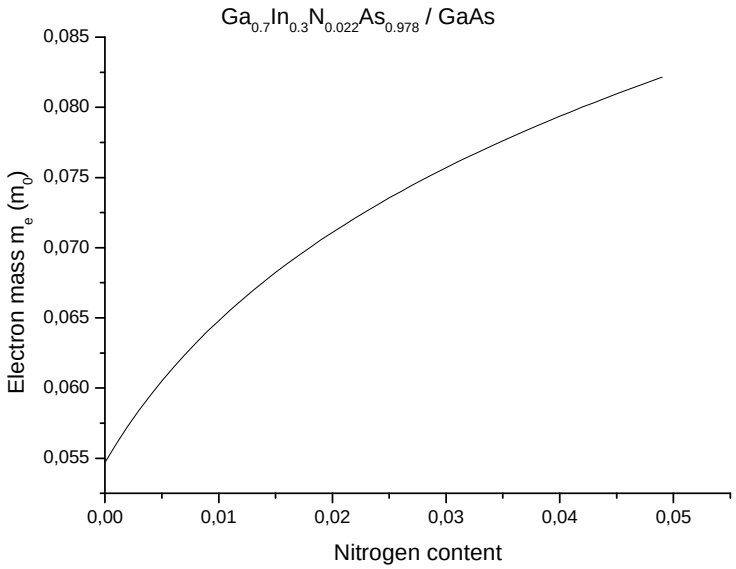

Figure 2.9 The calculated values of electron effective mass with increasing nitrogen concentration.

Such an increase of effective mass as a function of nitrogen content in GaInNAs system may be beneficial for device designing due to its effect on subband carrier populations.

2.8. Conclusions

In conclusion, theoretical models and corresponding calculations have been presented to show the unusual and fascinating properties of dilute nitrides. These unusual properties include the giant reduction of band gap energy with decreasing lattice constant, the appearance of the E_- and E_+ subbands in conduction band and a

strong increase of the electron effective mass with decreasing bandgap energy (increasing nitrogen composition).

CHAPTER 3

CRITICAL THICKNESS

3.1. Introduction

Nitrogen containing III-V ternary and quaternary alloys represent a novel material system which has many exciting properties and a great potential for many applications in optoelectronic and photonics. By far, the most studied and the best understood are the GaInNAs alloys with low nitrogen concentration, where impressive progress in the material growth and device fabrication has been achieved within a short time. To secure the full exploration of the alloy potential for device applications, compressive studies of basic band structure and recombination processes in materials have been undertaken. The majority of discovered fundamental physical properties can be referred to as unusual and fascinating. The orientation dependence is not examined theoretically until now. Therefore, we present, in this chapter, the orientation dependence of critical thickness and material parameters.

3.2. Orientation Dependence of Critical Thickness

In the growth of lattice-mismatched systems, a critical layer thickness h_c exists below which the strained layer is expected to be in a thermodynamically stable state. Above h_c , the misfit is predominantly accommodated by material defects such as dislocations. So, in a strained-layer, lattice-mismatched system, the thickness of QWs in the structure is a design constraint. Hence, the enhancement of h_c, if possible, would be of crucial importance for devices in lattice-mismatched systems [32]. Recently, Anan et al. [43] stated that the critical thickness is dependent on the growth direction, with the largest h_c expected for the (111) growth direction in zinc-blende systems. We review below the calculation of critical thickness h_c with respect to growth orientation.

The critical thickness h_c can be calculated by solving the following the Matthews and Blakeslee equation for a single heterostructure [43,44]:

$$Bbh_c\varepsilon_0\cos\theta = Db\left(1-\sigma\cos^2\alpha\right)\left[\ln\left(\frac{h_c}{b}\right)+1\right] \tag{3.1}$$

where B and D are constants concerned with elasticity defined below, b is the amplitude of the Burgers vector, ε_0 denotes misfit strain, and σ is the Poission's ratio. θ is the angle between the slip direction and that direction in the interface which is perpendicular to the line of intersection of the slip plane and the interface , while α is the angle between the dislocation line and the Burgers vector. The left-hand term denotes the force F_e due to strain which acts to form a misfit dislocation. The right-hand term denotes the line tension of a dislocation F_l which acts to resist the formation of dislocation [32].

Shown in Fig.3.1. is a representation, at an exaggerated scale, of the unit cells of $Ga_{1-x}In_xN_yAs_{1-y}$ and GaAs.

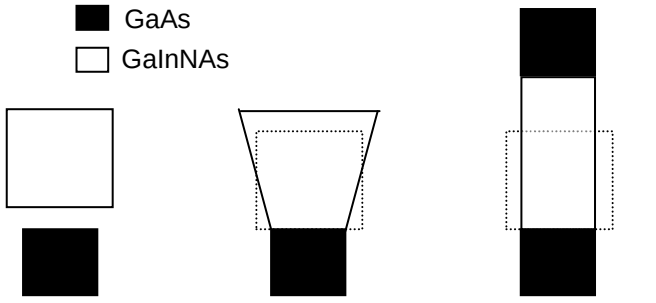

Figure 3.1 Schematic diagram (a) of separate $In_xGa_{1-x}As$ and GaAs unit cells, (b) a single strained layer $Ga_{1-x}In_xN_yAs_{1-y}$ structure, and (c) an inserted $Ga_{1-x}In_xN_yAs_{1-y}$-GaAs strained layer structure. Shown for reference, as a dashed line is the original $Ga_{1-x}In_xN_yAs_{1-y}$ cell shape.

The unit cell of $Ga_{0.7}In_{0.3}N_{0.022}As_{0.978}$ can be as much as 1.7 % larger. In the case of a single layer, as shown schematically assuming a relatively thick GaAs host in Fig. 3.1(b), the $Ga_{1-x}In_xN_yAs_{1-y}$ cell is shortened in both directions parallel to the interface (biaxial compression) and elongated in the direction normal to the interface (uniaxial tension). If the force F_e exceeds the tention F_l in a dislocation line, migration of threading dislocation results in the formation of a single misfit dislocation [44].

If the $Ga_{1-x}In_xN_yAs_{1-y}$ cell is inserted between thick layers of the host to form a quantum well, then both interfaces are under biaxial compression, as shown in Fig.3.1(c). If the force F_e exceeds twice the tension F_l in a dislocation line, migration of threading dislocation results in formation of two misfit dislocations [44]. In the case of a superlattice, where the concept of a host does not apply and alternating layers are under either biaxial compression or tension [44].

The effect of growth orientation on h_c mainly consists of two parts [43]. The first is the dependence of elasticity on orientation, which is reflected through the change of coefficients for B, σ, and D in Eq.(3.1). The second is the change in geometrical arrangement of the Burgers vector and heterointerface, the effect of which is described by the change in the θ value of Eq.(3.1). The expressions for coefficients B, σ and G for the (001) and (111) directions are listed in table 3.1. Eq.(3.1) was simplified by Coleman [45] for the (001) orientation, assuming the layers in a superlattice to have equal elastic constants, as

$$h_c = \frac{a}{\kappa\sqrt{2}\pi\varepsilon_0}\frac{1-0.25\sigma}{1+\sigma}\ln\left(\frac{h_c\sqrt{2}}{a}+1\right) \qquad (3.2)$$

where a is the lattice constant of the strained layer, and σ^{001} is the (001) Poission ratio, κ is a coefficient having a value of 1 for a strained layer superlattice, 2 for a single quantum well and 4 for a single strained layer. In this thesis, Eq.(3.1) is used to calculate critical thickness.

	(001)	(111)
σ	$C_{12}/(C_{11}+C_{12})$	$(C_{11}+2C_{12}-2C_{44})/2(C_{11}+2C_{12}+C_{44})$
B	$(C_{11}+2C_{12})(C_{11}+C_{12})/C_{11}$	$6(C_{11}+C_{12})C_{44}/(C_{11}+2C_{12}+C_{44})$
G	$(C_{11}+C_{12})/2$	C_{44}
D	$G_0G_sb/[2\pi(G_0+G_s)(1-\sigma)]$	$G_0G_sb/[2\pi(G_0+G_s)(1-\sigma)]$

Table 3.1 The values of σ, B , G, and D in terms of the elastic constants. G_0 and G_s denote the shear moduli for the overgrown layer and substrate, respectively. D has the same notation for both orientations, but has a different actual value because of orientation dependence of G and σ.

Material parameters	GaAs	InAs	GaN	InN
Lattice Constant a_o ($\mathring{A}$)	5.6533	6.0584	4.50	4.98
a_c (eV)	-7.17	-5.08	-6.71	-2.65
a_v (eV)	-1.16	-1.0	-0.69	-0.7
Elastic Stiffness C_{11} (GPa)	1221	832.9	293	187
Elastic Stiffness C_{12} (GPa)	566	453.6	159	125
Elastic Stiffness C_{44} (GPa)	600	395.9	155	86.0
Deformation Potential b (eV)	-2.0	-1.8	-2.0	-1.2
Deformation Potential d (eV)	-4.8	-3.6	-3.7	-9.3
Electron Effective Mass m_c (m_o)	0.067	0.026	0.15	0.07
Energy gap E_g (eV)	1.424	0.417	1.94	3.299
γ_1	6.98	20.0	2.7	3.72
γ_2	2.06	8.5	0.76	1.26
γ_3	2.93	9.2	1.11	1.63

Table 3.2 Binary material parameters [29,46].

We compare in Fig. 3.2 the critical thickness of InGaAs/GaAs system for (001) and (111) orientations. As can be seen from Fig. 3.2 the calculated h_c on (111) is about two times larger than that on (001) over the entire indium composition range. This bring a benefit for the use of (111) oriented InGaAs/GaAs systems since the desired well width can be obtained safely without having dislocations or any other non-uniform structure.

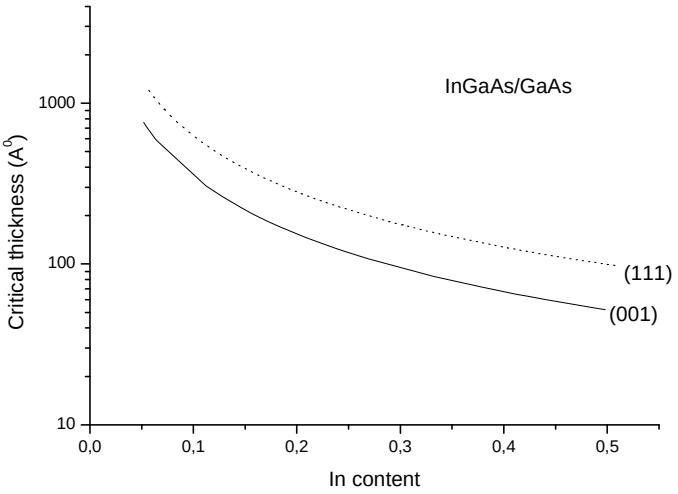

Figure 3.2 Comparison of the critical thickness of a strained quantum-well grown on (111) and (001) oriented substrates calculated for InGaAs as a function of indium composition, using the Matthews and Blakeslee model.

The main goal of this chapter, is to compare the orientation dependence of quaternary system of InGaNAs system with InGaAs. The critical thickness h_c increases with increasing nitrogen content in InGaNAs as shown in Fig. 3.3, but the increase of indium in InGaNAs causes a reduction in critical thickness, as shown in Fig. 3.4. This opposite behavior again can be of special importance.

As can be seen from Fig. 3.4 the critical thickness on (111) is nearly two times larger than that on (001) in InGaNAs/GaAs system. The difference is mainly caused by the different θ value between (001) and (111); i.e., $\cos\theta$=1/2 for (001) and $\cos\theta = 1/2\sqrt{3}$ for (111) [32]. This means that the force acting to form the misfit dislocation is $\sqrt{3}$ times larger for (001), thus resulting in a smaller h_c. It is seen that the critical layer thickness h_c in (111) oriented layers is more suitable compared to (001) oriented layers. This enhancement of the h_c in (111) oriented layers should enable layers of higher strain to be grown for a given well width. Therefore we may expect that this enhancement could lead to emission at longer wavelengths for laser grown (111) substrates [32].

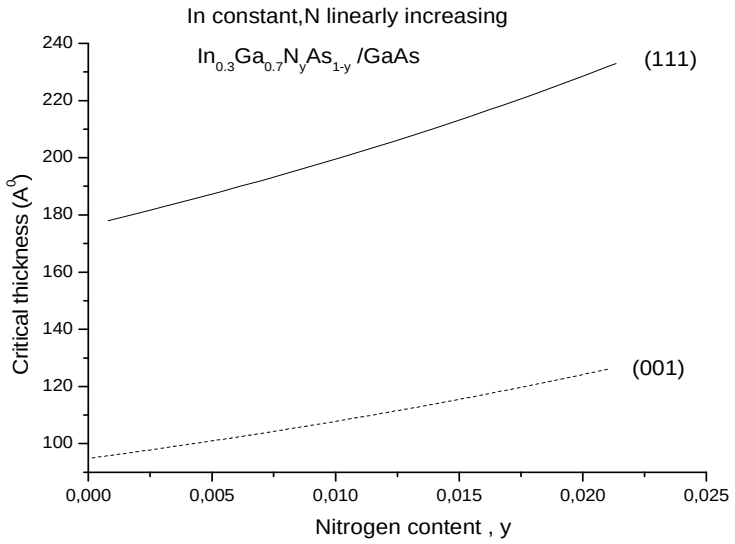

Figure 3.3 Comparison of the critical thickness of a strained quantum-well grown on (111) and (001) oriented substrates calculated for InGaNAs as a function of nitrogen composition, using the Matthews and Blakeslee model.

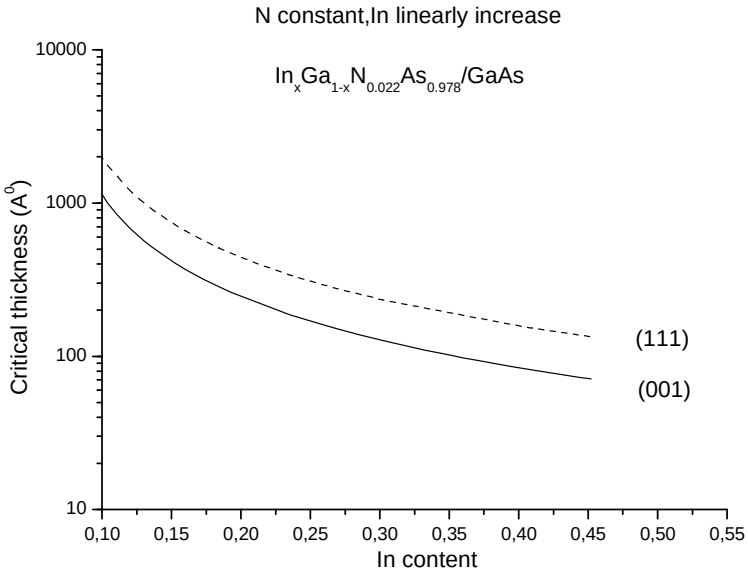

Figure 3.4 The critical thickness of a strained quantum-well grown on (111) and (001) oriented substrates calculated for InGaNAs as a function of indium composition, using the Matthews and Blakeslee model.

3.3. Orientation Dependence of Material Parameters

There are some fundamental differences in the orientation dependent material parameters between (111) and (001) bulk materials and between the quantum structures grown on these different oriented substrates. These difference will be presented in the next subsections [47].

3.3.1 Effective Masses of Holes

An important difference between quantum structures grown on (001) and (111) substrates is the different effective hole masses for these two orientations. The effective masses in the vicinity of the zone centre (k=0) are expressed in terms of Luttinger parameters (γ_1, γ_2 and γ_3) as follows [47]

$$m^*_{hh,lh} = \frac{m_0}{\gamma_1 \mu 2\gamma_2} \text{ for (001)}, \qquad m^*_{hh,lh} = \frac{m_0}{\gamma_1 \mu 2\gamma_3} \text{ for (111)}, \qquad \text{for perpendicular masses,} \tag{3.3}$$

$$m^*_{hh,lh} = \frac{m_0}{\gamma_1 \mu \gamma_2} \text{ for (001)}, \qquad m^*_{hh,lh} = \frac{m_0}{\gamma_1 \mu \gamma_3} \text{ for (111)}, \qquad \text{for parallel masses.} \tag{3.4}$$

where m_0 is the free-electron mass, the upper sign stands for heavy-hole, and lower for light-hole. Lawaetz [48] calculated Luttinger parameters for all the Ill-V compounds. However, detailed experimental investigations [49-52] show that Lawaetz Luttinger parameters for GaAs lead to a much larger heavy effective mass than is observed along the (111) direction [47]. So the Luttinger parameter set proposed by Vurgaftman [29,46] is used for GaAs in our calculations. Resultant hole effective masses for GaAs, InAs, InN and GaN are calculated and listed in Table 3.1. The material parameters for the ternary $In_xGa_{1-x}As$ are calculated by using the values of binary InAs and GaAs by interpolation technique. The heavy- and light-hole effective masses for an increasing nitrogen content are calculated by interpolation technique and are shown in Fig.3.5. It is seen from Fig.3.5 that the light-hole masses

for both (001) and (111) orientation is more or less the same for the whole range of nitrogen composition. So we can conclude that the light-hole effective masses has a weaker dependence on orientation. It is also seen from the same figure that the heavy-hole masses for the two orientation increases slightly with increasing nitrogen content.

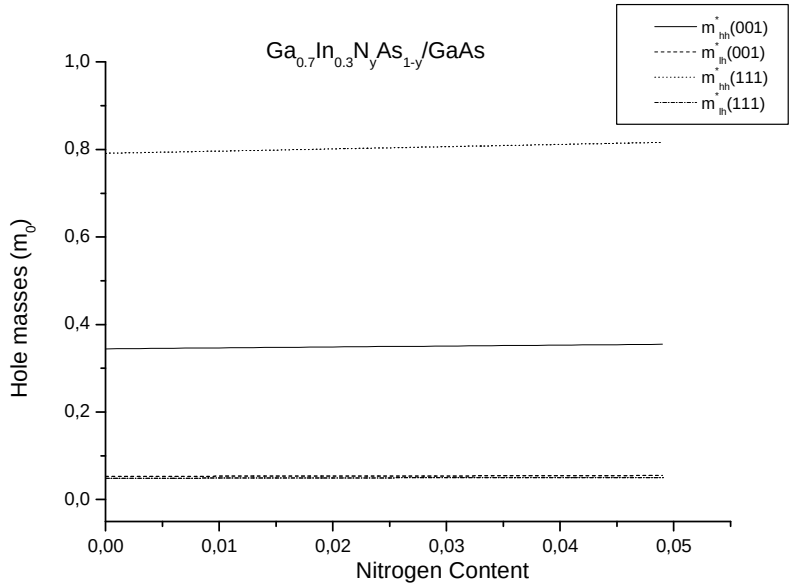

Figure 3.5 The calculated heavy-hole and light-hole masses for both (001) and (111) orientation as a function of nitrogen content.

However, the heavy-hole effective mass along the (111) direction is found to be about twice as that along (001). This causes the confinement energies of heavy-hole along (111) direction being smaller than that of (001) orientation for the same well parameters [47].

3.3.2 Elastic Deformation and Strain-induced Band-edge Shift

For a sufficiently thin epilayer, all of the strain will be incorporated elastically in the layer. Consider the case of a compressively-strained layer. The epilayer is under a biaxial stress, such that its in-plane lattice constant $a_{\|}$ equals that of the substrate a_s**.**

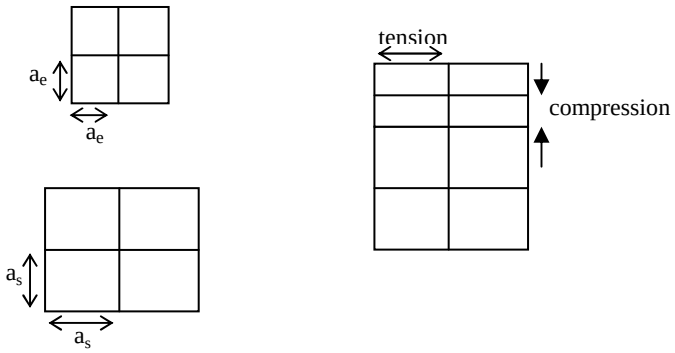

Figure 3.6 Illustration of the compression that results perpendicular to the growth direction for tension in the plane of the layers.

When the epilayer is grown on a (001) substrate, the perpendicular strain $\varepsilon_{\perp}$ is simply proportional to $\varepsilon_{\parallel}$, off-diagonal strain-tensor elements vanish, and the three major diagonal elements, ε_{ij} (i = x, y, *z*), can be expressed as [47]

$$\varepsilon_{xx} = \varepsilon_{yy} = \frac{a_s - a_e}{a_e} = \varepsilon_{\parallel} \equiv \varepsilon_0 \tag{3.5}$$

$$\varepsilon_{zz} = -\frac{2C_{12}}{C_{11}}\varepsilon_0 = -\frac{2\sigma^{(001)}}{1-\sigma^{(001)}}\varepsilon_0, \tag{3.6}$$

where a_e and a_s are respectively the lattice constants of the epilayer and substrate material, C_{11} and C_{12} are the elastic stiffness constants, and ε_0 is the strain which, increases with indium composition. The constant σ is known as Poisson's ratio, which is given as

$$\sigma = \frac{C_{11}}{2C_{12}}, \tag{3.7}$$

Since there is no stress in the growth direction it can be simply shown for a strained layer grown on an (001) substrate [53-54] that the different components of the strain tensor are given by

$$\begin{aligned} \varepsilon_{xx} &= \varepsilon_{\parallel}, \quad \varepsilon_{yy} = \varepsilon_{xx}, \quad \varepsilon_{zz} = \varepsilon_{\perp}. \\ \varepsilon_{xy} &= 0, \quad \varepsilon_{yz} = 0, \quad \varepsilon_{xz} = 0. \end{aligned} \tag{3.8}$$

It is important to note that for (001) growth, the strain tensor is diagonal while for non-(001) directions, the strain tensor has nondiagonal terms [47].

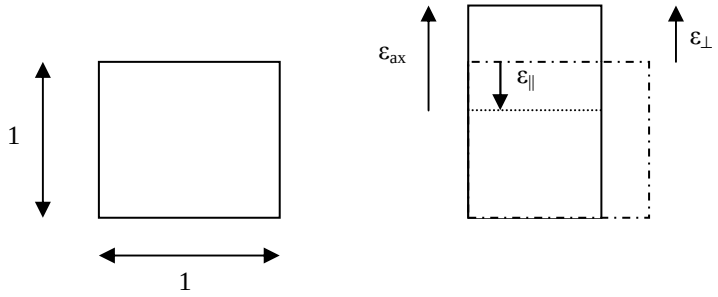

Figure 3.7 Illustration of strain decomposition for the case of biaxial compression in a cubic crystal. The unit cell on the left compresses in the plane ("||" direction) by a fractional amount, $\varepsilon_{\parallel}$, giving an increase in "height" $\varepsilon_{\perp}$. The axial strain, ε_{ax}, is the amount by which the crystal is extended in the "⊥" direction compared to the height it would have had (short dashed).

The total strain can be resolved into a purely axial component, ε_{ax}

$$\varepsilon_{ax} = \varepsilon_{zz} - \varepsilon_{xx} = -\left(\frac{C_{11} + 2C_{12}}{C_{11}}\right)\varepsilon_0, \tag{3.9}$$

and a hydrostatic component ε_{vol} $\left(= \frac{\Delta V}{V}\right)$

$$\varepsilon_{vol} = \varepsilon_{xx} + \varepsilon_{yy} + \varepsilon_{zz} = 2\left(\frac{C_{11} - C_{12}}{C_{11}}\right)\varepsilon_0, \tag{3.10}$$

Therefore, there are two types of modifications that occur in the strained layer. The first effect is due to a change in the volume of the unit cell, known as the hydrostatic component, which gives rise to a change in the mean band gap ΔE_g by amount

$$\Delta E_g = (a_c - a_v)\,\varepsilon_{vol} \tag{3.11}$$

where a_c and a_v are the hydrostatic deformation potential of the conduction- and the valance-band, respectively [47].

The second, more important effect is due to the tetragonal deformation of the cubic crystal, which splits the degeneracy of the light and heavy-hole states at the valence-band maximum [55]. For small axial strain, the heavy and light-hole states are shifted by an energy ± S respectively, with respect to the mean valence-band edge energy. The magnitude of S, the strain-splitting energy, is dependent on the axial strain [47].

$$S = -b\,\varepsilon_{ax} \tag{3.12}$$

where b is the axial deformation potential. For compressive strain, the heavy hole levels are brought to the top of the valence band while tension strain brings the light-hole levels to the top of the valence band. A positive value of the S corresponds to biaxial compressive strain and a negative strain value of S to biaxial tensile strain.

For (111) growth, the tetragonal distortion is with respect to the (111) direction, not the cubic axes; consequently, the off-diagonal strain-tensor elements are nonzero in this case. In the (111) oriented strained system, the strain tensor elements ε_{ii} and ε_{ij} are given by [56]

$$\varepsilon_{ii} = \frac{4C_{44}}{C_{11} + 2C_{12} + 4C_{44}}\varepsilon_{0,} \tag{3.13}$$

$$\varepsilon_{ij} = \frac{-(C_{11} + 2C_{12})}{C_{11} + 2C_{12} + 4C_{44}}\varepsilon_{0,} \tag{3.14}$$

where (i,j = x,y, z, i≠j). The band-edge shift for (111) quantum structures is related to the shear component of the deformation potential, d, due to the non-zero off-diagonal strain-tensor elements. Thus, the uniaxial and hydrostatic component of the strain are given as

$$S = \sqrt{3} d\varepsilon_{ij} \quad , \tag{3.15}$$

$$\Delta E_g = 3 (a_c - a_v) \varepsilon_{ii} \tag{3.16}$$

3.4 Change in the Valence Band-edge for the two Orientations

The strain tensor elements for the (001) and (111) orientations are different. This result in a smaller Poisson ratio for (111) oriented growth, and consequently larger hydrostatic shifts compared to (001), yielding a strong orientation dependence to the energy difference between the conduction- and valence-bands. The hydrostatic and uniaxial strain corrections to the Γ point energy differences between the conduction- and valence bands for (001) and (111) are given respectively by [47],

$$\Delta E_{hh,lh} = -2a\left(\frac{C_{11} - C_{12}}{C_{11}}\right)\varepsilon_0 \pm b\left(\frac{C_{11} + C_{12}}{C_{11}}\right)\varepsilon_0, \tag{3.17}$$

$$\Delta E_{hh,lh} = -3a\varepsilon_{ii} \; \mu \sqrt{3} d\varepsilon_{ij} \tag{3.18}$$

where ΔE_{hh} and ΔE_{lh} are the shifts in the heavy-hole and light-hole valence-band edges with respect to the conduction-band edge. Table 3.2 gives the material parameters necessary to calculate Eqn. (3.15) and Eqn (3.16) for InGaAs strained layers on GaAs. The parameters for the ternary ($In_xGa_{1-x}As$) and quaternary ($Ga_{1-x}In_xN_yAs_{1-y}$) quantum-wells are constructed from a linear interpolation of the endpoint binary semiconductors, InAs, GaN, InN and GaAs. The calculated variation in energy for the heavy- and light-hole valence band edges is shown for $In_xGa_{1-x}As$ in Fig. 3.8 for (001) and (111) orientation. The heavy- and light-hole valance band energies for $In_xGa_{1-x}As$ is increasing with indium composition. A similar diagram is obtained for $Ga_{1-x}In_xN_yAs_{1-y}$/GaAs system and shown in Fig.3.9. It is seen from Fig.3.9 that the heavy- and light-hole band edge energies in $Ga_{1-x}In_xN_yAs_{1-y}$/GaAs decreases with increasing nitrogen concentration. This decrease is due to the lattice parameter variation which is decreasing with nitrogen composition and increasing with indium composition. This is an important difference between $In_xGa_{1-x}As$ and $Ga_{1-x}In_xN_yAs_{1-y}$.

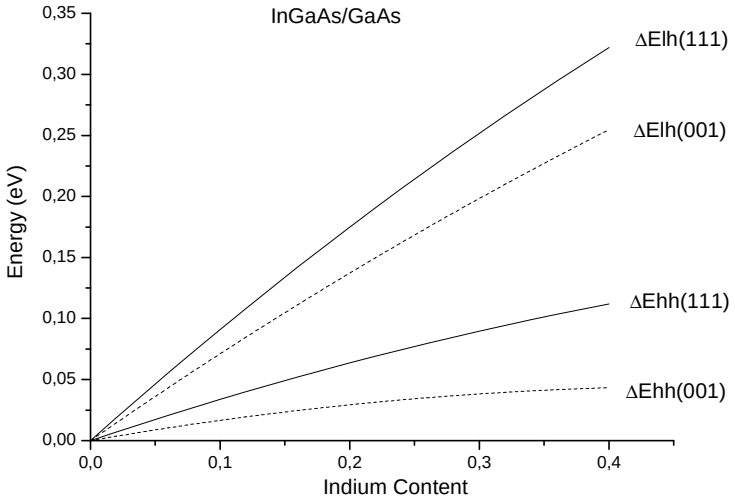

Figure 3.8 The shift in the heavy-hole valence band edge (ΔE_{hh}) and light hole valence band edge (ΔE_{lh}) with respect to the conduction band edge for (001) and (111) orientation as a function of In composition for $In_xGa_{1-x}As/GaAs$ strained layers.

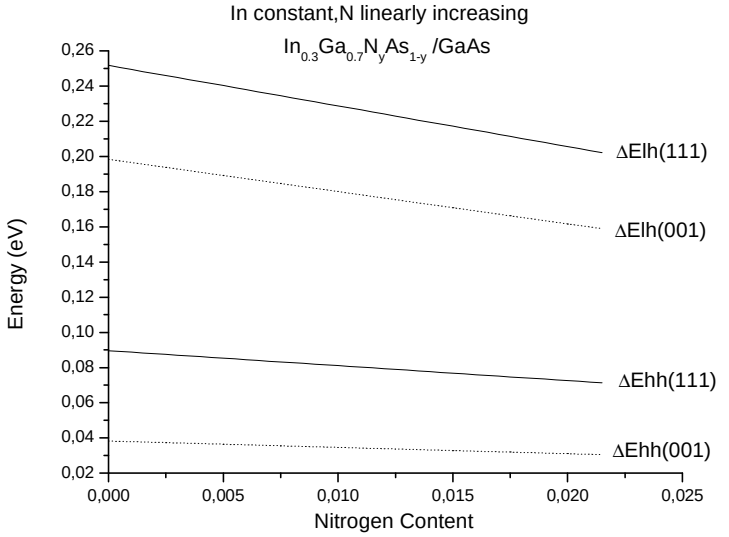

Figure 3.9 The shift in the heavy-hole valence band edge (ΔE_{hh}) and light hole valence band edge (ΔE_{lh}) with respect to the conduction band edge for (001) and (111) orientation as a function of nitrogen composition for $Ga_{1-x}In_xN_yAs_{1-y}/GaAs$ strained layers.

The shift of the heavy-hole and light-hole valence-band edge with composition is greater on (111) than on (001) for InGaAs/GaAs system. This leads to a larger band gap on the (111) orientation for a given composition compared to (001) orientation. This enhancement of the band gap is mostly due to the hydrostatic pressure component of the strain. For tetrahedral semiconductors generally [47],

$$C_{11} \approx 2C_{12}, \qquad C_{12} \approx C_{44} \tag{3.19}$$

so that for (111) growth;

$$\varepsilon_{ii} \approx -\varepsilon_{ij} \approx \tfrac{1}{2}\,\varepsilon_0 \tag{3.20}$$

Therefore, a comparison of the hydrostatic pressure component of strain on (001) and (111) orientation shows that the hydrostatic pressure component of strain is 1.5 times larger on the (111) than (001) orientation for InGaAs/GaAs system.

3.5 Conclusions

In this chapter, we have firstly compared the critical thickness of InGaAs and InGaNAs as a function of In and N concentrations for both orientation of (001) and (111). We have calculated that the critical thickness of InGaAs/GaAs laser system decreases with increasing indium concentration for both (001) and (111) direction. In addition, it was calculated that the critical thickness in (111) orientation is greater than that of the (001) orientation. Same variation is also obtained for InGaNAs/GaAs system with one exception; the magnitude of the critical thickness increased with the addition of nitrogen. This behaviour can be of special interest since one can grow strained layers of InGaNAs safely due to high critical thickness.

We have secondly concluded that light-hole mass is independent from both orientation and nitrogen concentration. On the other hand, heavy-hole mass on (111) orientation is calculated as being twice of that of the (001) orientation. This increased mass on (111) orientation decreases the confinement energies of heavy-holes in (111) orientation.

We have finally obtained that the change in the valence-band edges behaves oppositely for indium and nitrogen concentrations; an increase of indium increases the valence band edges whereas an increase of nitrogen decreases the valence-band edges.

CHAPTER 4

A COMPARATIVE ANALYSIS of InGaAs/GaAs and InGaNAs/GaAs QW LASER STRUCTURES WITH RESPECT TO GROWTH ORIENTATION OF (001) and (111)

4.1 Introduction

The oldest but the best developed and still most sophisticated heterostructure laser system is the AlGaAs/GaAs system. AlAs and GaAs systems have the same lattice constants. This allows the design of any structure, with any combination of layer compositions, without regard to lattice mismatch or the associated dislocation formation. The range of wavelengths available from lattice-matched AlGaAs/GaAs quantum well heterostructure laser is from $\lambda \approx 0.88 - 0.65$ μm. After AlGaAs/GaAs, the best studied semiconductor heterostructure laser materials system is InGaAsP/InP. High quality InP substrates are less readily available and more expensive so InGaAsP/InP quantum well heterostructure lasers are far less common. The range of wavelengths available from lattice-matched InGaAsP/InP quantum well heterostructure lasers is from $\lambda \approx 1.1\text{-}1.6$ μm. These wavelength ranges are sufficient to cover many important applications such as the use of modulated InGaAsP/InP lasers at $\lambda \approx 1.55$ μm as sources for low loss, minimum dispersion optical fiber communication links, and the use of high power AlGaAs/GaAs laser arrays at $\lambda \approx 0.82$ μm for solid state lasers. But there is an obvious wavelength range of $\lambda \approx 0.88\text{-}1.1$ μm. This range is unavailable in any III-V lattice-matched heterostructure laser materials system. There are, however, a number of important applications that require laser emission in this range including frequency doubling of wavelengths near the 1.06μ m emission wavelength of Nd:YAG solid state lasers and pumping the upper states of rare-earth-doped silica fiber amplifiers.

An examination of the available direct gap III-V compound semiconductor alloys suggests that perhaps the best material system for obtaining emission wavelengths in the range $\lambda \approx 0.88\text{-}1.1$ μm is $In_xGa_{1-x}As$. There is, however, no suitable binary substrate material that allow lattice-matched composition of $In_xGa_{1-x}As$ in the wavelength range of interest. Thus, only a heterostructure materials system in which a very large mismatch must be accommodated (ε_0 as great as 3 %) may be considered.

Much of the current epitaxy focuses on the (001) substrate orientation because of wide range of growth conditions, which results in good epitaxial layer quality on this crystalline orientation. We study in this thesis the potential benefits of growing unstrained lasers, and strained using growth directions other than the conventional (001) direction. The highest valence band is highly anisotropic, even in unstrained bulk III-V semiconductors, where the heavy hole mass is approximately twice as large along (111) as along (001) [50]. This increases the number of heavy-hole confined states and the energy separation between the highest heavy and light hole states for a given well width. It has recently been shown that (111) GaAs/AlGaAs unstrained lasers can have lower threshold current density than equivalent (001) lasers [57,58]. Ghiti et al. [59] described laser gain calculations, which shows that this improvement is consistent with the different valence subband structures associated with the two growth directions.

Tao and Wang [60] demonstrated for the first time a strained InGaAs QW laser grown on (111) GaAs at a wavelength of 988 nm with a threshold current density of 267 *A*/cm^2. Then Ishihara and Watanabe [61] succeeded in fabricating a strained InGaAs quantum well laser on (111) GaAs with emission wavelength of 1072 nm and threshold current density of 164 *A*¢m ^{2}. Smith and Mailhiot [62] predicted that due to lack of inversion symmetry in the zinc-blende structure, a net displacement of the positive and negative charges can be generated in a strained quantum well grown on a (111) substrate. As a result, if growth of strained zinc-blende semiconductors occurs away from the (001)-like directions, a large strain-induced internal electric field emerges via the piezoelectric effect [63]. The existence of this strain induced electric field across the well

i) Tilts the energy band structure modifying the carrier wave functions,

ii) Confines the electron and hole wave functions to opposite sides of the well leading to a decrease in the wave function overlap, and

iii) Pushes electron confined states to lower energies and the hole confined states to higher energies resulting in a decrease of the lowest transition energy.

These points have been illustrated in Fig. 4.1.

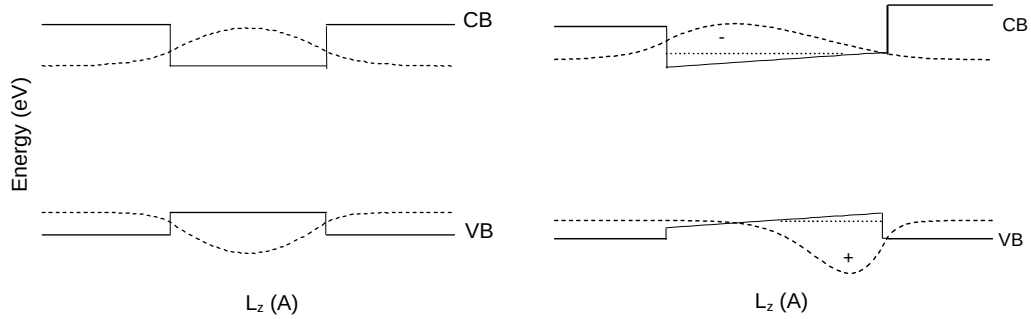

Figure 4.2 Conduction, valence band edges and carrier wavefunctions for quantum wells grown along (001) and (111) oriented substrates.

Furthermore, the built-in field can be compensated by applying an external field [64] or by photogenerated electron-hole pairs [65,66]. These pairs are spatially separated by piezoelectric field and forms two planes of opposite charge. This in turn induces an electric field that partially cancels (screens) the built-in field. The extend of this screening will clearly depend on the density of electrons and holes. This carrier-dependent field effect has some potential application for nonlinear devices where the free carriers are generated by photo-absorption.

In addition, the critical thickness of strained $In_xGa_{1-x}As$ layers grown on (111) GaAs is believed to be about twice that for (001) [24]. This enhancement of the critical layer thickness allows an increase of the In content in (111) strained In_xGa_{1-x} As quantum well lasers, which could in principle lead to emission at longer wavelengths on (111) substrates than that of (001) substrates.

Communication systems based on optical fiber are working in the 1.3-1.5 μm, corresponding to the second and third optical windows, respectively. This kind of lasers are very extended, but the InGaAsP/InGaAs/InP material system has some intrinsic properties that do not allow to achieve high performance laser emission, for example, the low conduction band offset, that make the carriers be poorly confined, and absence of materials to grow high quality Bragg reflectors on top of these structures.[67] The new material InGaNAs [67] solves these problems, since AlGaAs system can be grown virtually lattice-matched to the GaAs substrate, and the conduction band discontinuity is large due to the large redsifth introduced by adding nitrogen to these layers. Successful laser emission has been already been demonstrated for the InGaNAs material. Despite its advantages, there are some difficulties in the growth and fabrication of InGaNAs based optoelectronic devices that must be overcome. For example, the degradation of this material due to the transition to the Stranski-Krastanov (3D) growth mode or the reduction in its optical properties when nitrogen is added to the InGaAs layers. Many of these problems of the InGaNAs layers can be solved when using GaAs (111) substrates. The suppression of the 3D growth mode in these kind of substrates, together with possible higher value for the critical layer thickness and the presence of a piezoelectric field in strained heterostructures grown on (111) [43] make this kind of orientation a suitable candidate to the development of optoelectronic devices working in the optical communication windows. Besides, the presence of a piezoelectric field for strained heterostructure grown on (111) makes this substrate orientation an interesting field for study, and could open device engineering possibilities.

In this chapter we calculate and compare the allowed energy levels and the corresponding wavefunctions for both (001) and (111) growth InGaAs/GaAs and InGaNAs/GaAs laser material systems. These calculations take into account the orientation dependent material parameters of effective mass, elastic deformation and strain-induced band-edge shift.

4.2 Energy Levels and Wavefunctions

The quantized energy levels and their corresponding wavefunctions for the carriers in the conduction and valence band are determined numerically by solving Schrödinger's equation of

$$-\frac{\eta^2}{2m^*}\frac{d^2\psi(z)}{dz^2}+[V_r(z)+V_F(z)]\psi(z)=E\psi(z), \tag{4.1}$$

for a quantum well of width L_z using the finite difference method [57]. ψ is the carrier envelope wavefunction, m^* is the carrier effective mass, $V_r(z)$ is the potential due to the quantum well, and $V_F(z)$ is the tilted potential due to the strain-induced built-in piezoelectric field for non-(001) oriented materials which is given by

$$V_F(z)=\pm eFz. \tag{4.2}$$

$V_F(z)$ is set to zero for (001) orientation.

4.2.1 Well Width Dependence of Confined Energy Levels in (001) and (111) Orientations

Figure 4.2 shows the calculated energy levels for electrons as a function of well with for (001) and (111) growth for InGaAs/GaAs and InGaNAs/GaAs lasers system by means of solving Schrödinger's equation. We kept the barrier thickness as constant. The confined energies get closer to the bottom of the well i.e. they get smaller, as the well width becomes thicker as it is seen in Fig.4.2.

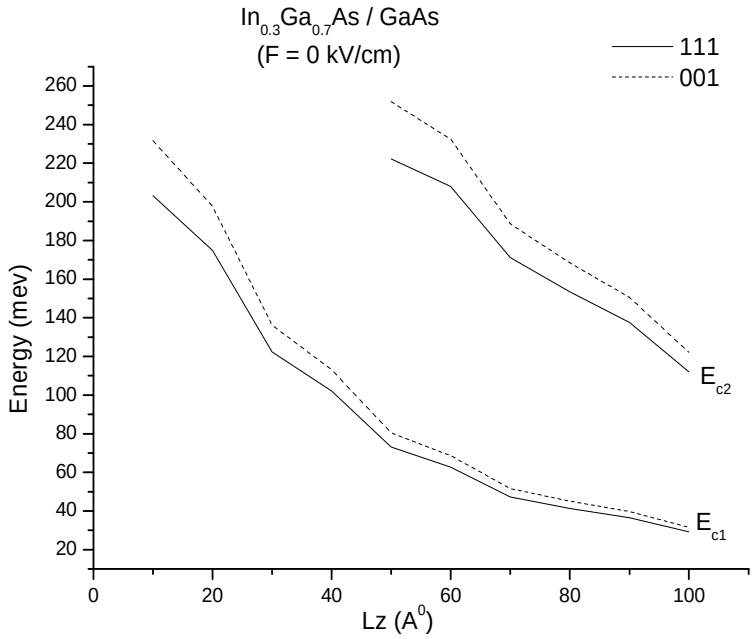

(a) InGaAs /GaAs

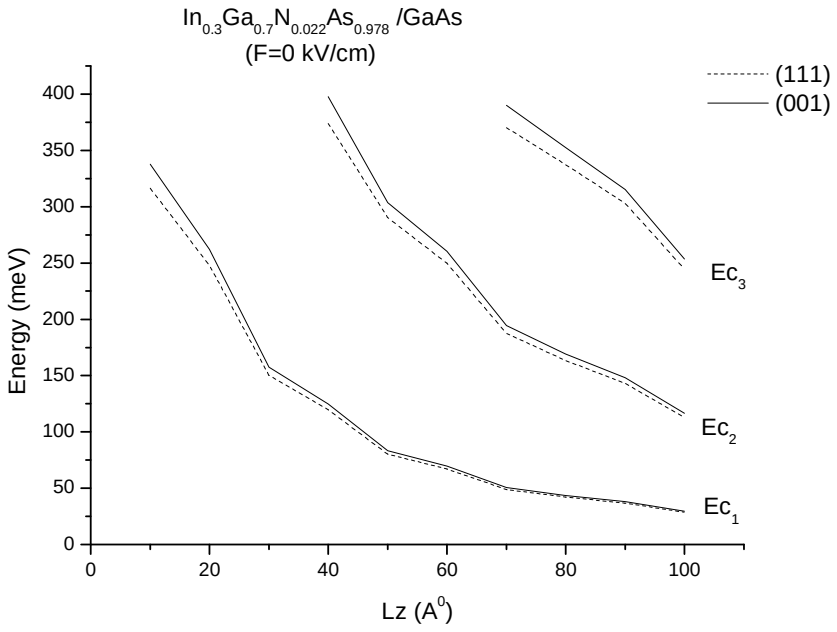

(b) InGaNAs / GaAs

Figure 4.2 Calculated quantized electrons energy levels of InGaAs and InGaNAs for the for (001) and (111) growth.

This section provides a comparison of the confined energy levels of electrons in InGaAs/GaAs and InGaNAs/GaAs alloys;

1. The confined energy levels in conduction band for (001) orientation is greater than (111) orientation for both N-free and N-included systems. However, the difference between (001) and (111) orientation is greater in N-free InGaAs/GaAs laser system.

2. The magnitude of the confined energy levels of conduction band gets bigger when N is added to InGaAs system. This is especially remarkable at narrow well widths. The difference between conduction band confined energy levels is small at wider well widths.

3. As it is clear from Fig.4.2 that the number of confined states increases with increasing well width.

The comparison of Fig.4.2(a) with Fig.4.2(b) reveals the fact that the number of confined electron states for InGaNAs/GaAs alloy is bigger than that of the InGaAs/GaAs alloy for a fixed well width.

Fig.4.3(a) and Fig.4.3(b), compares the confined heavy- and light-hole states for (001) and (111) orientation and for InGaAs/GaAs and InGaNAs/GaAs systems. As can be seen from Fig.4.3(a) and (b) there are more confined hole states on (111) orientation for a fixed well width due to the increase in the perpendicular hole mass in (111) orientation as we have mentioned in section 3.3.1. The presence of more energy levels brings a disadvantage because one has to inject more and more carriers to achieve population inversion and this in turn increases the threshold current density which we do not want.

Fig. 4.3 also provides the comparison of the nitrogen dependence of (001) and (111) orientation. Fig. 4.3(a) reveals the fact that addition of N into InGaAs system has almost no effect on valence band structure on (001) orientation. There are only minor changes in confined energy levels.

	γ_1	γ_2	γ_3	$m_{\Gamma 6}$	$m^*_{\perp\ hh}$ (001)	$m^*_{\perp\ lh}$ (001)	$m^*_{\perp\ hh}$ (111)	$m^*_{\perp\ lh}$ (111)
$In_{0.4}Ga_{0.6}As$	10.89	3.99	4.81	0.067	0.345	0.053	0.791	0.048
$In_{0.3}Ga_{0.7}N_{0.022}As_{0.978}$	10.71	3.92	4.73	0.072	0.349	0.053	0.802	0.049

	$m^*_{\parallel\ hh}$ (001)	$m^*_{\parallel\ lh}$ (001)	$m^*_{\parallel\ hh}$ (111)	$m^*_{\parallel\ lh}$ (111)
$In_{0.4}Ga_{0.6}As$	0.0672	0.1449	0.0637	0.1645
$In_{0.3}Ga_{0.7}N_{0.022}As_{0.978}$	0.0684	0.1473	0.0648	0.1672

Table 4.1 Conduction-band edge effective mass $m_{\Gamma 6}$ and calculated perpendicular and parallel hole effective masses for (001) and (111) orientations using the Luttinger parameters from Vurgaftman [29] for GaAs and Lawaetz for InAs [48].

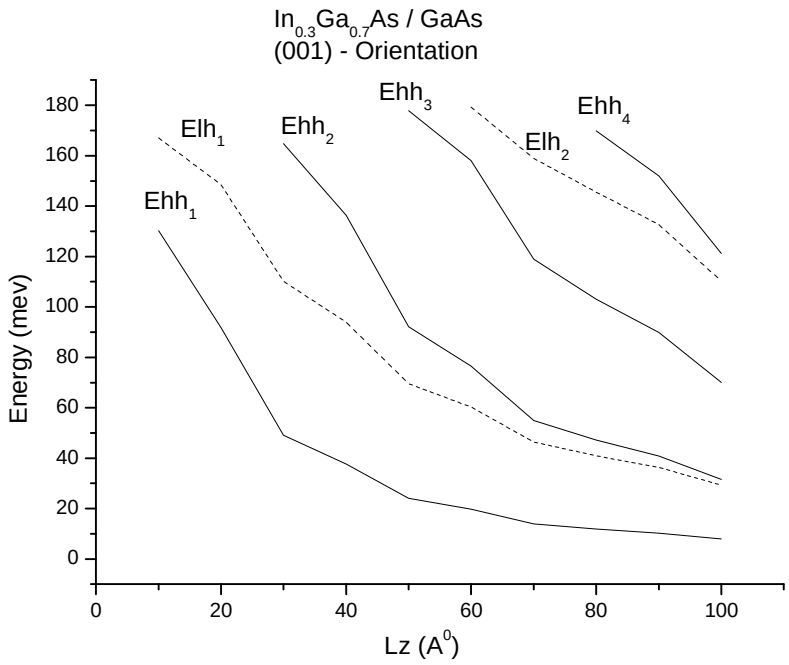

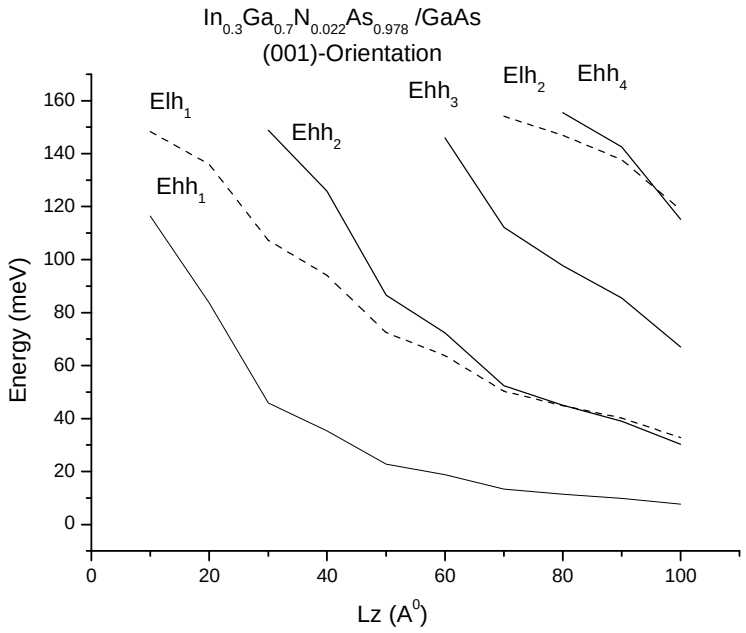

(a) (001) oriented

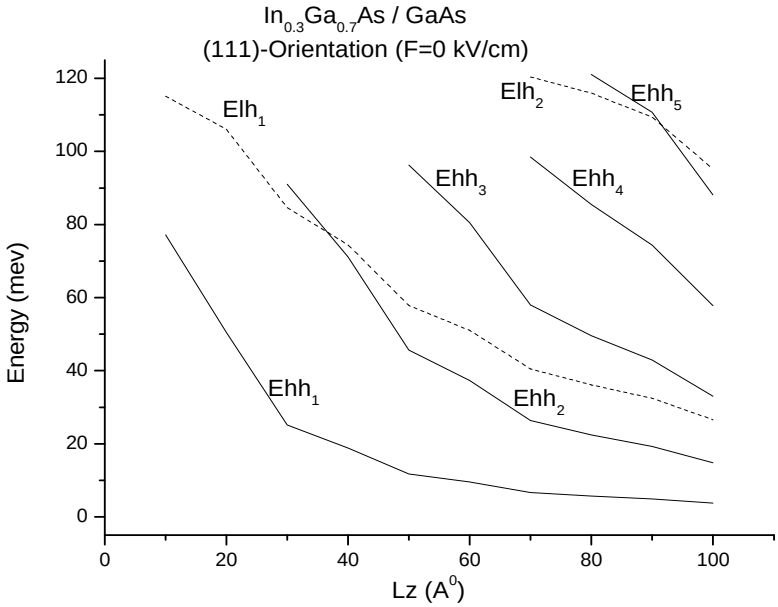

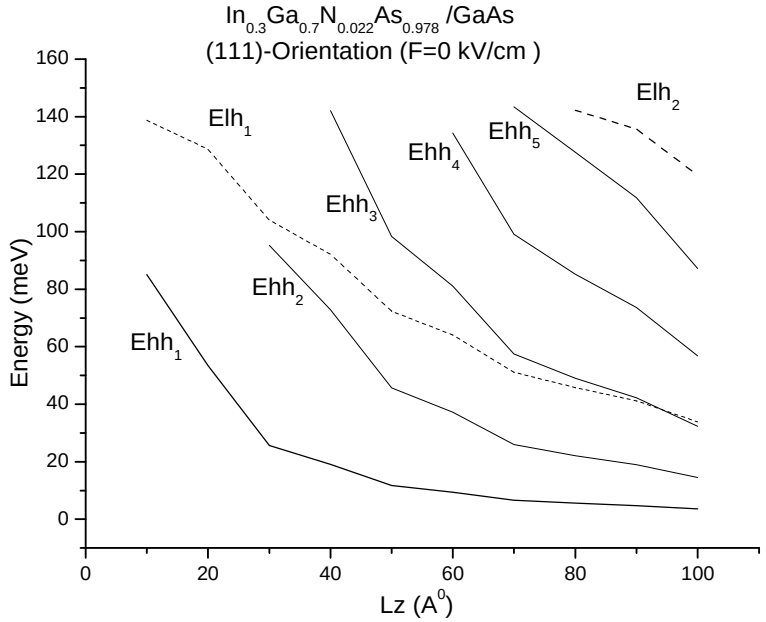

(b) (111) oriented

Figure 4.3 The confined heavy- and light-hole states for (001) and (111) orientation of InGaAs and InGaNAs systems as a function of well width.

4.2.2 Indium and Nitrogen Dependence of Confined Energy Levels in (001) and (111) Orientation

We want to investigate the confined energy levels for electrons and holes as a function of increasing nitrogen and indium content in both orientations of (001) and (111). Fig.4.4 shows this comparison for confined energy levels of electrons.

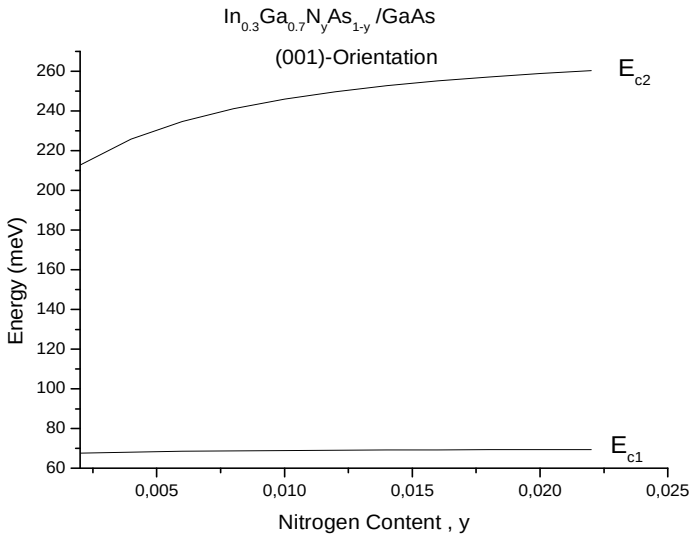

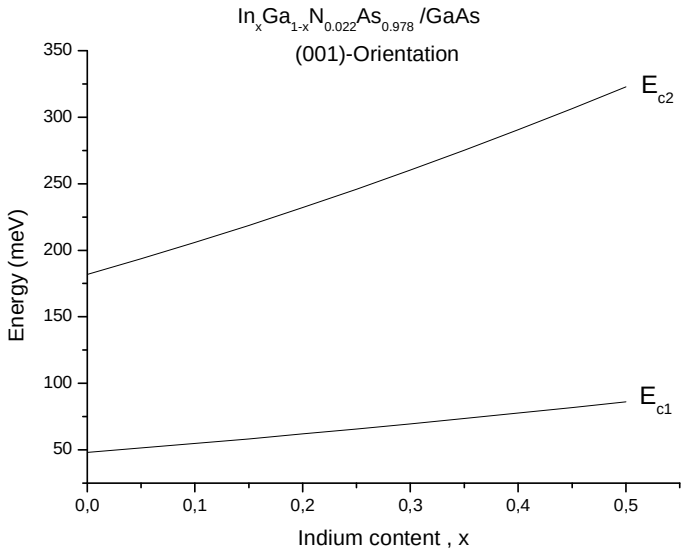

(a) (001) orientation

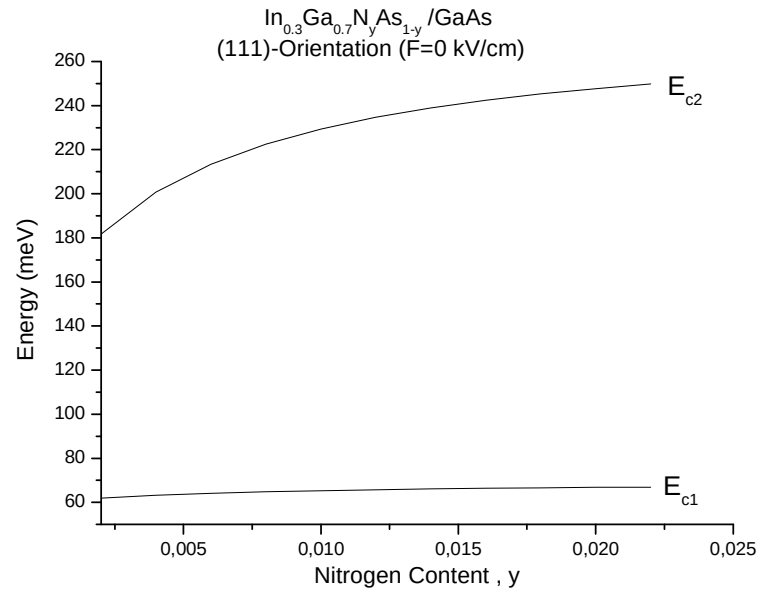

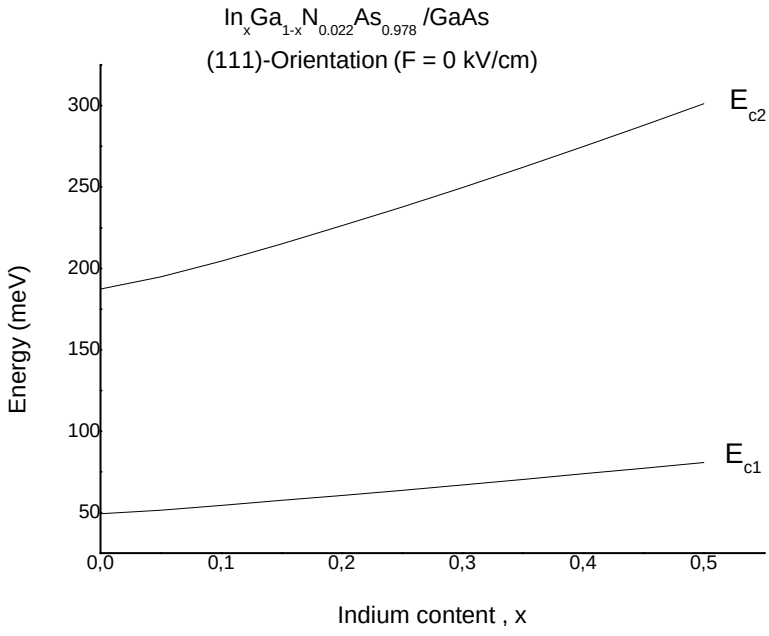

(b) (111) orientation

Figure 4.4 The confined electron states in conduction band for (001) and (111) orientation of InGaAs and InGaNAs systems as a function of nitrogen and indium content.

Fig. 4.4 shows that if the nitrogen content increases in InGaNAs alloy on (001) orientation, the first energy level of conduction band increases very slightly whereas a quicker increase in the energy level is calculated for the second energy level of conduction band. On the other hand, the confined energy levels of first and second conduction band increases significantly when indium content increases. Similar trends are also calculated for (111) orientation as shown in Fig.4.4(b). However, the increase in (001) orientation is faster compared to that of the (111) orientation.

We now want to present the indium and nitrogen content dependence of valence band confined energy levels for (001) and (111) orientation. As can be seen from Fig.4.5(a), the confined state of first heavy-hole is almost nitrogen independent in (001) orientation. On the other the higher levels increases with increasing nitrogen content. Confined energy levels of InGaNAs strongly depends on the indium concentration in (001) orientation.

It is obvious that there are more confined levels in (111) than that of the (001). The nitrogen and indium dependence of confined energy levels in (111) orientation behaves similarly with that of the (001) orientation as shown in Fig.4.5(b).

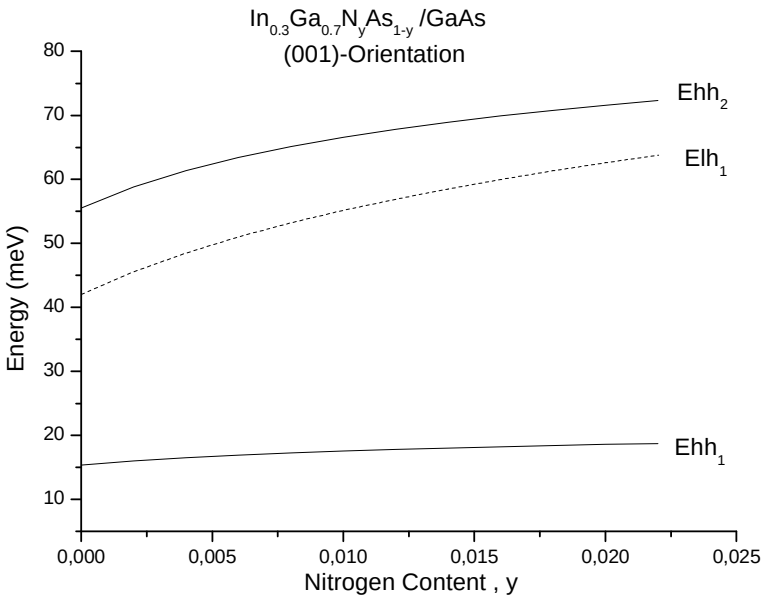

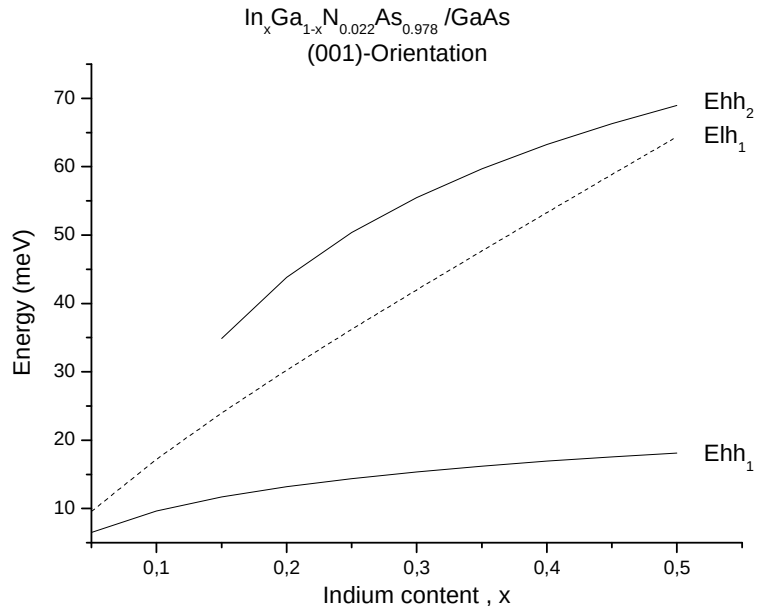

(a) (001) orientation

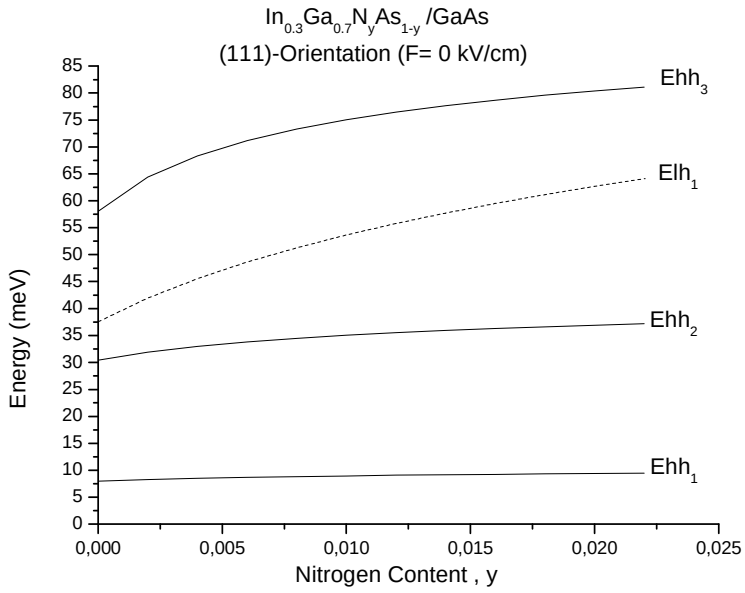

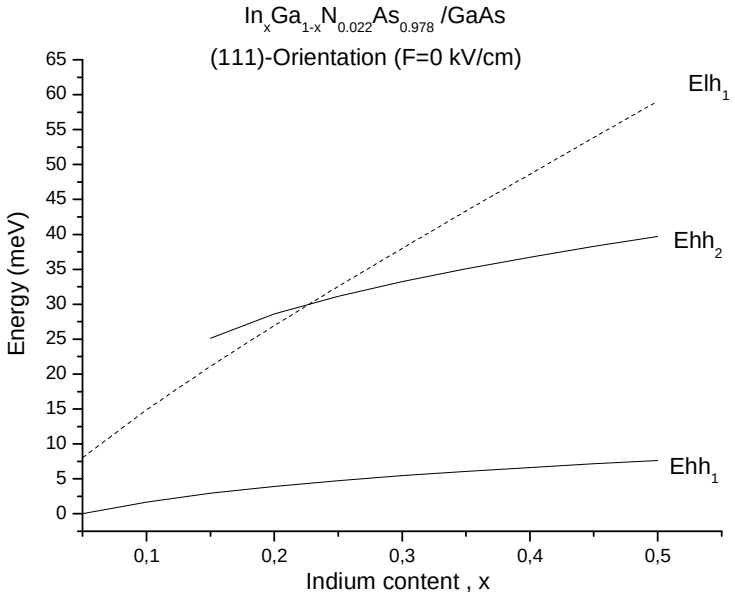

(b) (111) orientation

Figure 4.5 The confined heavy and light-hole states in valence band for (001) and (111) orientation of InGaAs and InGaNAs systems as a function of nitrogen and indium content.

4.2.3 The Effect of the Internal Piezoelectric Field on the Confined Energy Levels and Wavefunctions

The presence of the internal piezoelectric field perturbs the quantum well potential energy profile from that of a symmetric finite square well to that of a highly asymmetric well (see Fig.4.1) with a corresponding finite tunnel barrier and the electron and hole wavefunctions are pinned against opposite to the quantum well heterointerfaces. This effect is illustrated in Fig.4.6(a)-(d). As can be seen from Fig.4.6, the wavefunction of the first confined electron state is pushed to left and the wavefunction of the first confined heavy-hole state is pushed to the right of the quantum well gradually when the field increases from 0 to 120 kV/cm. As a consequence of this, the oscillator strength for the n=1 electron to heavy-hole (e-hh) exciton is decreased significantly compared to the zero electric field case (flat-band case).

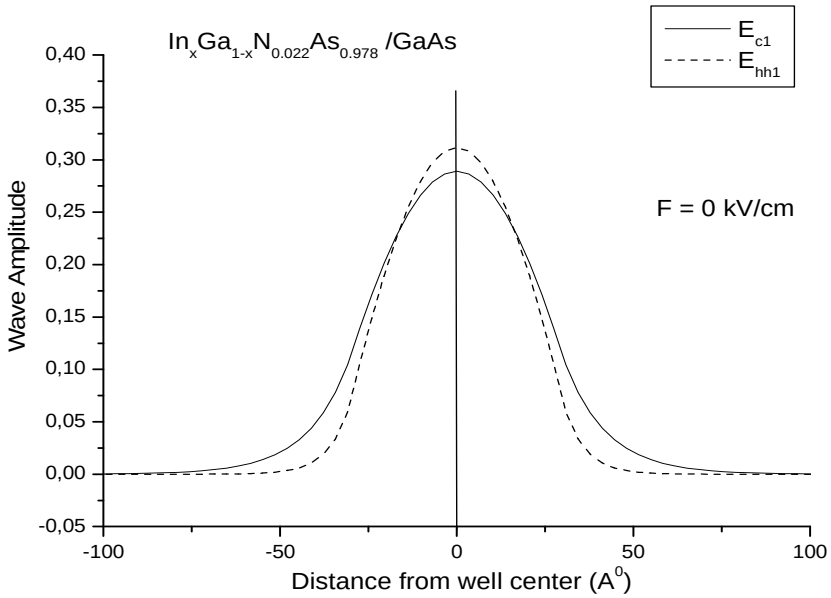

(a) No Applied field

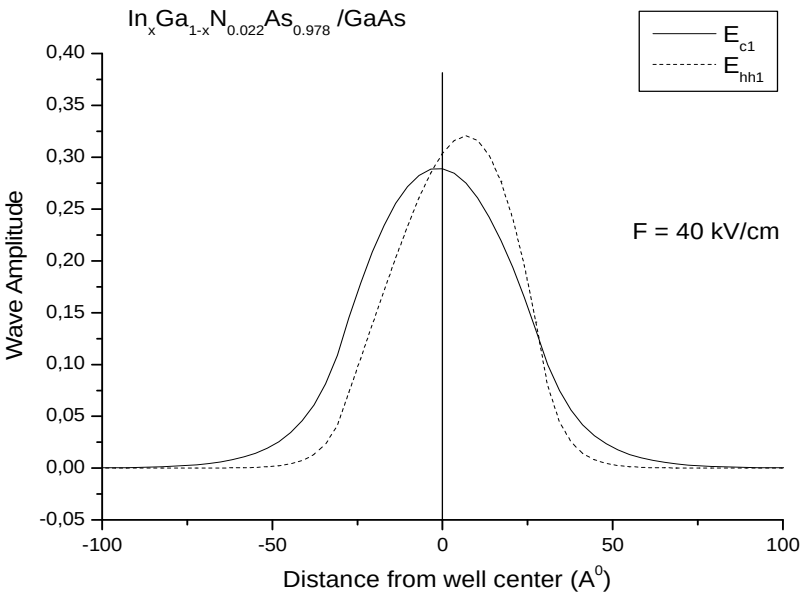

(b) F = 40 kV/cm

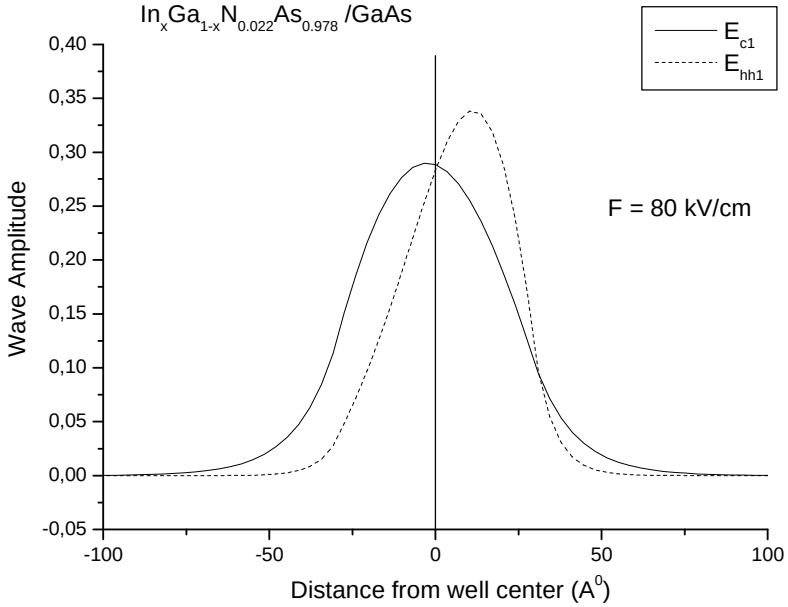

(c) F = 80 kV/cm

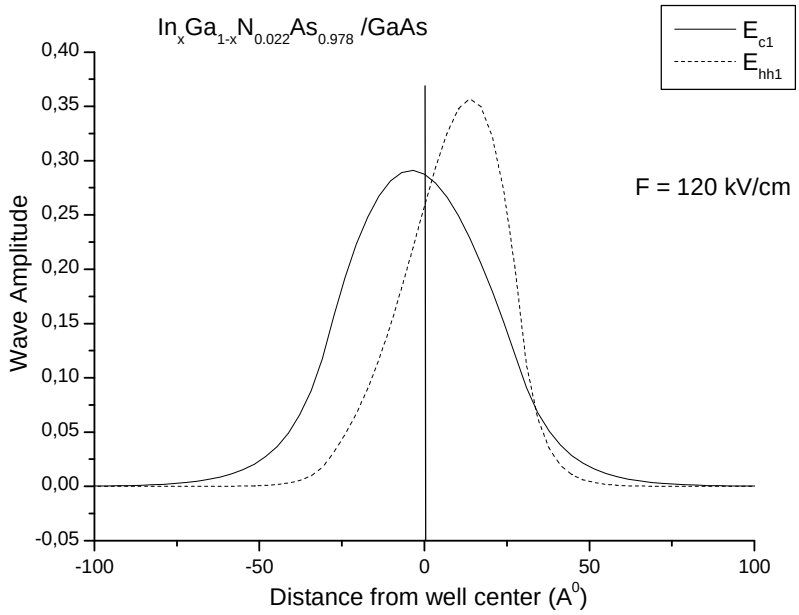

(d) F = 120 kV/cm

Figure 4.6 Wavefunctions for the first confined electron state in conduction band and the first confined heavy-hole state in valence band in a quantum well in the presence of an internal piezoelectric field.

As a consequence of the movement of the electron wavefunctions to one end and the hole wavefunctions to the other end, due to the piezoelectric field, the transition energy is lowered relative to the zero electric field case. This can be seen from a closer examination of Fig.4.7(a) for a fixed value of the well depth.

The comparison of the variation of the confinement energy of the electron and hole in Fig.4.7a and b for a fixed band-offset value reveals that the energies of the both heavy-holes and electrons shift to the bottom of the well as a function of the electric field.

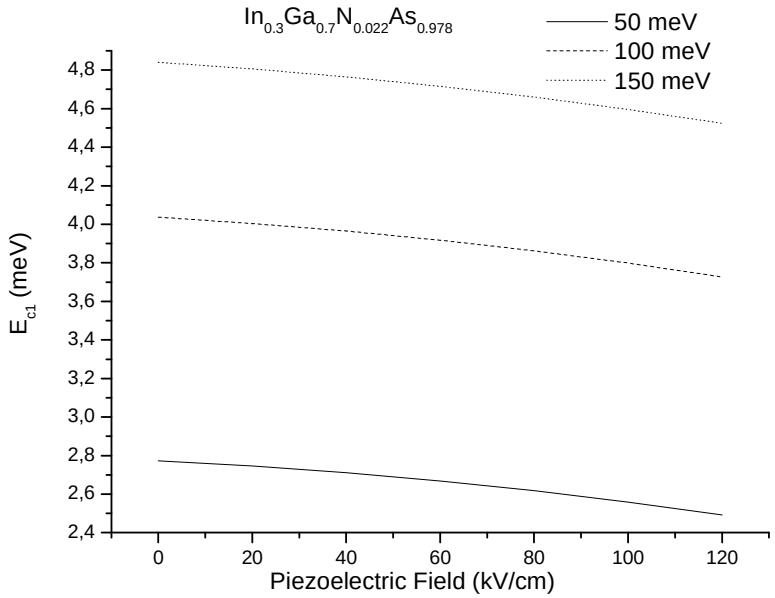

(a)

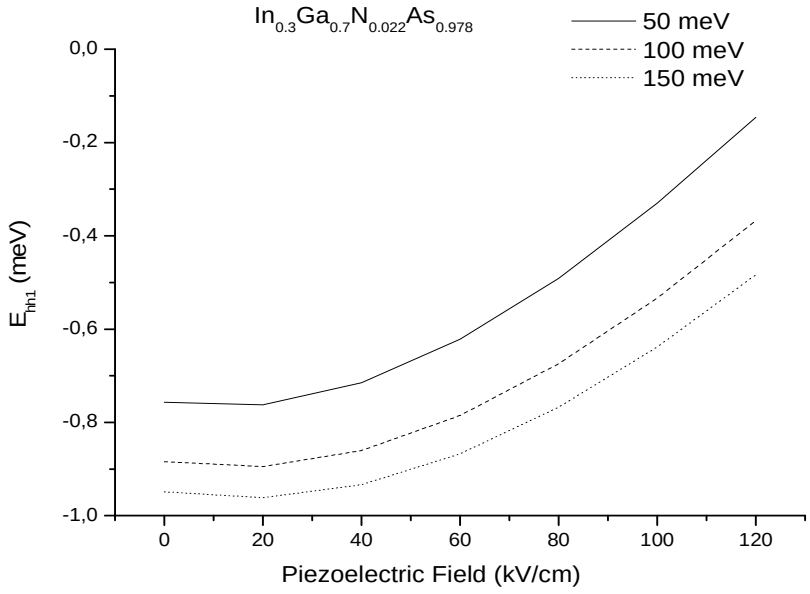

(b)

Figure 4.7 The confinement energies of both first electron- and hole-states as a function of piezoelectric field for different band-offsets (well-depths).

It is seen that the E_{c1} values decreases with increasing internal piezoelectric field for a fixed ΔE_c, i.e. E_{c1} values gets closer to the bottom of the well. A similar variation is obtained for the first heavy-hole state, and again it is seen that the E_{hh1} gets closer to the bottom of the well for a fixed valence-band-offset value, ΔE_v. This illustrates that the transition energy of the (e1-hh1) exciton is lowered with increasing internal field.

Fig.4.7 provides also the effect of the magnitude of the band offets on the confined energy levels. It can be concluded from Fig.4.7(a) and Fig.4.7(b) that the increase in magnitude of the band-offsets increases the confinement energies of both electron- and hole-states. The increase of magnitude of the band-offsets also causes the amplitude of the wavefunctions to get bigger. This brings an advantage, since the carrier confinement to the well gets better when the wells get deeper. This is shown in Fig.4.8 shows the calculated wavefunctions for the first heavy-hole state as a function of an internal piezoelectric fields for different values of valence band-offsets. The band offset determines the depth of the corresponding well.

As an overall, we have shown that, in the presence of an internal piezoelectric field across the InGa(N)As layers in (111) orientation, the e1-hh1 exciton is lowered compared to their (001) counter parts.

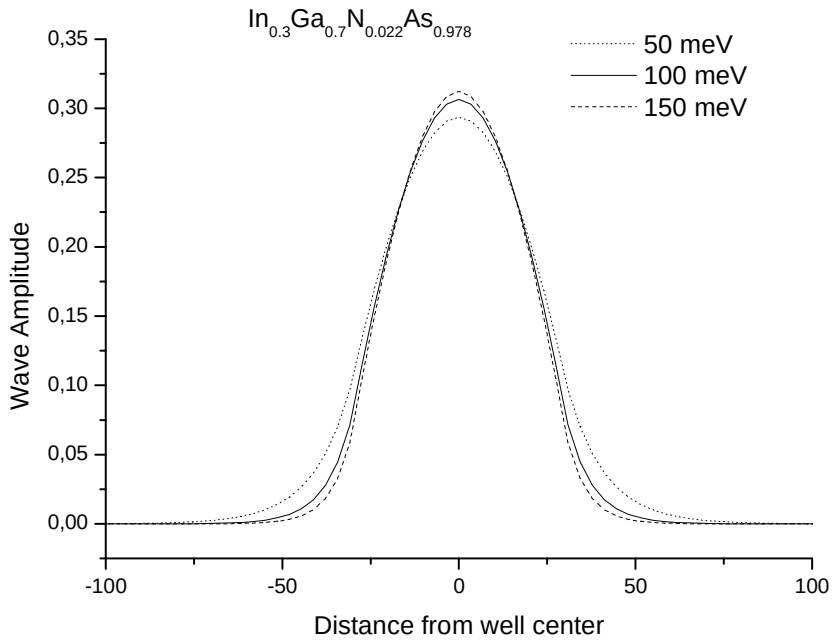

(a) No Applied Field

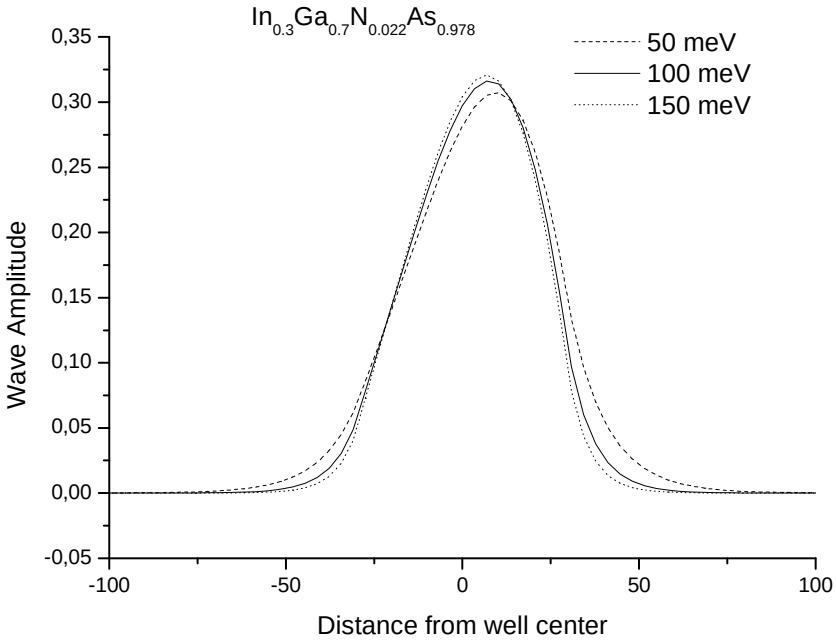

(b) F = 40 kV/cm

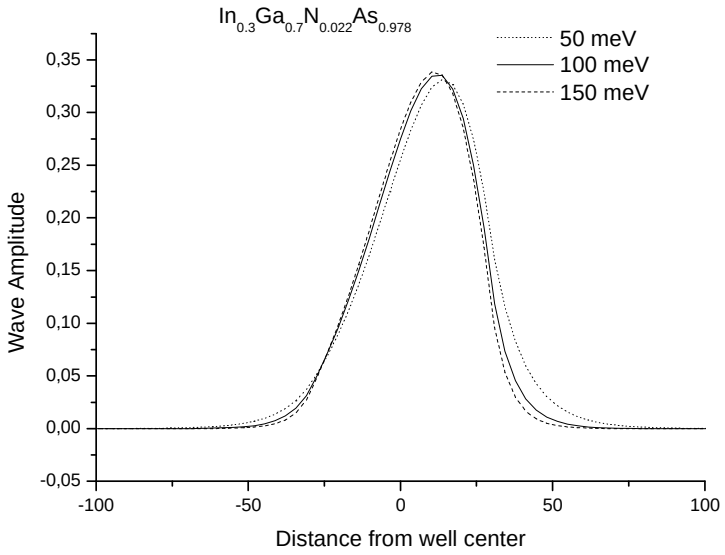

(c) F = 80 kV/cm

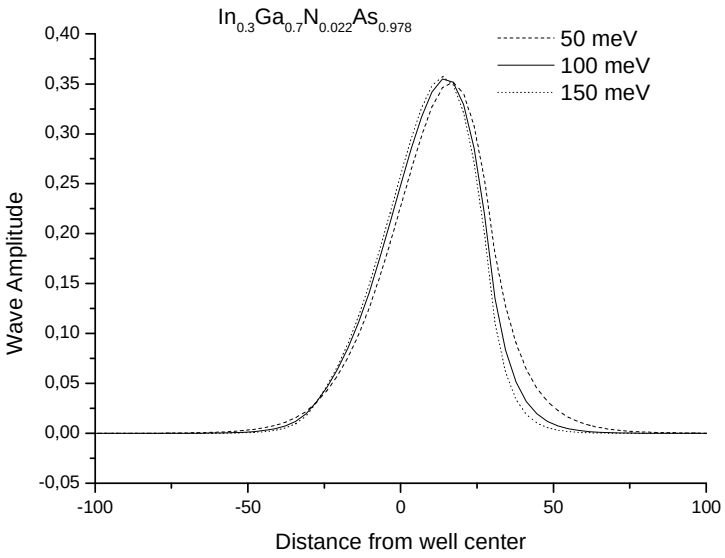

(d) F = 120 kV/cm

Figure 4.8 The amplitude of the confined energy level of first heavy-hole state, E_{hh1}, with increasing piezoelectric field for three different values of valence-band-offset, ΔE_v .

As can be seen from Fig.4.9 the shift in the confinement energy of the first heavy-hole state is the greatest for the largest field and wider wells. A similar variation is obtained for the electron state as well. So, the changes in the first e-hh exciton transition is expected to be more dramatic for a wide quantum well than that of a narrow well due to the greater spatial separation between the centroids of the electron and hole wavefunctions.

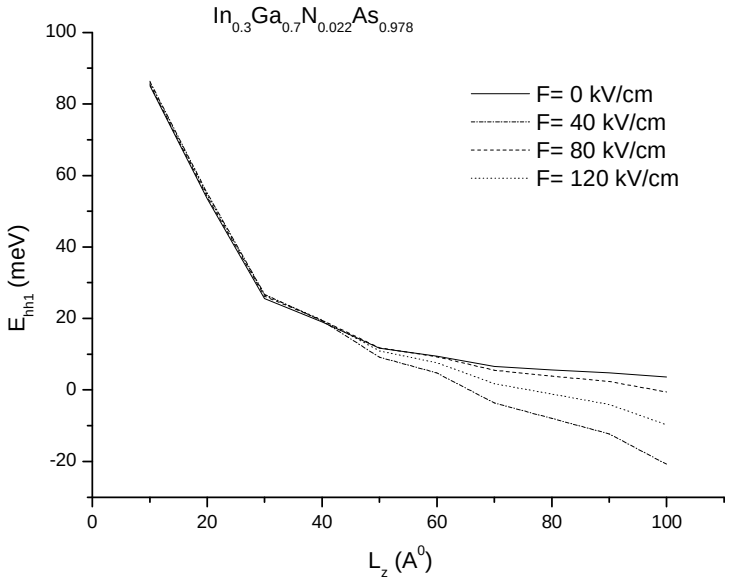

Figure 4.9 The shift in the confinement energies of the first heavy-hole state.

4.3 Conclusions

The detailed analysis of well width dependence of confined energy levels for N-free and N-included system in the two growth orientations has shown that te confined energy levels of conduction band of nitrogen free system is dependent on the growth direction, the N-included system is almost growth direction independent. On the other hand, the confined levels of valence band is orientation dependent for both N-free and N-included system. The confined levels of valence band increases in (111) direction due to the increased hole masses both in N-free and N-included system.

In addition, we have calculated that the confined energy levels of electrons are strongly dependent on indium concentration in both (001) and (111) direction. The electron energy levels increases rapidly with increasing indium content. This increase is faster in (001) orientation than that of (111) orientation. On the other hand a weaker nitrogen dependence is calculated for both directions.

The composition dependence of valence band energies have shown that the hole energies increases with both with nitrogen and indium compositions. Our calculations revealed that confined hole energies is strongly dependent on indium concentration in both orientation direction.

The calculations of the wavefunctions of the first confined energy levels of conduction- and heavy-hole band with the existing piezoelectric field in (111) direction have illustrated that electron and hole wavefunctions pinned to opposite sides of the quantum well with increasing piezoelectric field. This brings a disadvantage compared to flat band case due to the decrease of oscillator strength.

The analysis of the effect of the internal piezoelectric fild on the first confined energies of conduction- and heavy-hole band reveals the fact that the first transtion energy is lowered with increasing piezoelectric field.

We have also analysed the effect of the magnitude of band-offsets on confined energies and seen that confined state energies get bigger with increasing band-offsets. The increase in the band-offsets, i.e. when the wells get deeper, the magnitude of the wavefunctions gets bigger.

We have finally shown that the reduction in energy level of the first exciton state is greater for internal piezoelectric fields and wider well widths.

CHAPTER 5

CONCLUSIONS

A lot of electronical devices work with laser system. Especially communication systems based on optical fiber are working properly in the 1.3-1.55 μm, so emitters have been investigated to have a good quality and cheap cost. The InGaAs(P)-InP material system is the most commonly used semiconductor laser system for optical telecommunication applications with emission wavelengths of 1.3 and 1.55 μm. However, the practical applications of InGaAs(P)-InP based lasers have been obstructed by its poor characteristics. One of the major problems is the thermal property, which is related to the low potential barrier height in the conduction band [68,69]. For example, the threshold current increases steeply with temperature, and the maximum operating temperature becomes limited. This can be explained by the presence of various loss mechanisms of Auger recombination [70], intervalence band absorption [71], and carrier leakage due to the small electron confinement [72]. To overcome these problems alternative improved materials have been sought for future sources in optical communication systems. One such material is AlGaInAs/InP, and another strong potential candidate is GaInNAs/GaAs based lasers. AlGaInAs/InP strained multiple quantum well (MQW) lasers have been developed to improve the temperature dependence in the 1.3 and 1.55 μm lasers by using wide bandgap barriers for the suppression of the thermal leakage [73,74]. These proplems have been solved, after the pioneering work of Kondow et al. [66], who proposed and grew the material, a number of research groups [75,76] have since demonstrated diode laser operation using InGaNAs quantum,well (QW) lasers. This material has attracted attention by virtue of its unusual physical properties compared to that of the conventional III-V compounds [77]. The novel material system, GaInNAs on a GaAs substrate [67,78], has several important advantages compared to the most commonly used InGaAsP/InP systems [77]. First of all, a better high temperature performance of the laser structures is achieved due to a larger

conduction band offset and, thus, it has improved electron confinement and decreased electron spill out at room temperature and above. Second, the increase of the electron effective mass with the addition of nitrogen provides a close match between the effective mass values for electrons and holes, which is beneficial for laser applications. In addition, GaInNAs gives the flexibility of tailoring the bandgap and an increase in the lattice parameter. Hence GaInNAs offers the potential for producing a material lattice matched or mismatched to GaAs with a wide range of bandgap energies[77] (from ≈ 1.5 eV to less than 0.8 eV) [79]. This provides a possibility of using a low cost GaAs substrate as a viable alternative to the dominating InP based heterostructure lasers. It has shown previously [80] that reduced Auger recombination also occurs in GaInNAs/GaAs, as a result of the larger electron effective mass. In these alternative systems of AlGaInAs/InP and GaInNAs/GaAs, the conduction band offset ratio is greater than 0.5, which is expected to lead to a stronger electron confinement. Therefore, these result in the lasing properties of these new materials becoming less temperature dependent than that of the InGaAsP/InP lasers [77].

Up to now extensive work has been developed on (001) GaInNAs/ GaAs QWs, allowing for laser diodes emitting at 1.3 μm to be obtained. However, much work remains to be done on (111) growth direction. The work carried out in this thesis considered the effect of nitrogen doping on the GaInAs and compared the two orientation systems of (001) and (111). The comparison of nitrogen-free system is also provided.

The lattice constant of N free system increases with increasing In content causing a decrease in bandgap decreases with increasing In content. On the other hand the increase in nitrogen fraction in quaternary material of GaInNAs causes a decrease in lattice parameter and a reduction in the bandgap which is an unusual property. In addition, unlike other conventional alloy semiconductors, the electron effective mass increases when the energy bandgap is reduced by adding nitrogen. This has a profound influence on the strength of electron-photon and electron-electron interactions.

It has been calculated that the critical thickness increases with increasing nitrogen content in III-N-V system. It has also been calculated that the critical thickness for strain relaxation is greater in (111) growth direction compared to (001) direction. So nitrogen based systems on (111) direction is better than that of nitrogen-free system on (001) direction from critical thickness point of view.

The hole masses in GaInNAs slightly increases with increasing nitrogen content for both (001) and (111) orientation, so the valence band masses can be considered as nitrogen independent for both (001) and (111) direction. We have calculated that the light-hole mass is orientation independent. On the other hand, we have seen that the heavy hole mass on (111) direction is found to be twice that of the (001) direction.

We have analysed the indium and nitrogen dependence of strain-induced band-edge shift of heavy-hole and light-hole band for (001) and (111) direction. It is seen from our calculations that valence band edge shift is more remarkable in (111) direction. On the other hand, the addition of indium and nitrogen cause different behaviors; the addition of indium increases the band edge shifts whereas the addition of nitrogen decreases the band-edge shifts. Therefore, the band-edge energies gets smaller in GaInNAs providing longer wavelengths compared to that of nitrogen-free InGaAs.

The hole-confined energy levels for (111) orientation is greater than (001) orientation for both N-free and N-included systems. However, the difference between (001) and (111) orientation is greater in N-free InGaAs/GaAs laser system. Addition of N into InGaAs system has almost no effect on valence band structure on (001) orientation. There are only minor changes in confined energy levels. If the nitrogen content increases in InGaNAs alloy on (001) orientation, the first energy level of conduction band increases very slightly whereas a quicker increase in the energy level is calculated for second energy level of conduction band. On the other hand, the confined energy levels of first and second conduction band increases significantly when indium content increases, similar trends are calculated for (111)

orientation. The increase of confinement energy of e^-'s with indium content is faster in (001) orientation compared to (111) orientation

The confined state of holes increase slightly with increasing nitrogen content. Confined energy levels of InGaNAs strongly depends on the indium concentration in (001)orientation. In addition, there are more confined levels in (111) than that of the (001) due to the heavier mass in (111) orientation. The nitrogen and indium dependence of confined energy levels in (111) orientation behaves similarly with that of the (001) orientation.

In order to compare the position of wavefunctions in (001) and (111) direction, we have calculated the wavefunctions of the first conduction- and heavy-hole state, keeping in mind that the flat band disappears due to the presence of piezoelectric field in (111) orientation. The calculated wavefunction of the first confined electron state is pushed to left and the wavefunction of the first confined heavy-hole state is pushed to the right of the quantum well gradually when the field increases from 0 to 120 kV/cm. As a consequence of this, the oscillator strength for the n=1 electron to heavy-hole (e-hh) exciton is decreased significantly compared to the zero electric field case (flat-band case). This brings a disadvantage since threshold current increases.

We have seen that the increase in internal piezoelectric field causes a decrease of the valance and conduction confined states which further decreases the first transition energy thereby increasing emitted photon wavelength. The analysis of band-offsets on confined energy levels and amplitude of wavefunctions have shown that both confined energy levels and wavefunctions get bigger with increasing band-offset, i.e. deeper wells.

We have finally shown that, the reduction of the energy level of the first exciton state increases with increasing internal piezoelectric fields and wider well widths.

REFERENCES

[1] Esaki, L. and Tsu, R. (1970). *IBMJ. Res*. Dev. **14**, 61.

[2] Jayaraman, V., Goodnough, T.J., Beam, T.L., Ahedo, F.M., Maurice, R.A. (2000). *IEEE Photon. Technol. Lett*. **12,** 1595.

[3] Kondow, M., Kitatani, T., Nakatsuka, S. Larson, M.C., Nakahara, K., Yazawa, Y., Okai, M., Uomi, K. (1997). Select. Topics Quantum Electron. *IEEE J.* **3,** 719.

[4] Kondow M., Uomi K., Hosomi K. and Mozume T. (1994). *Japan J. Appl. Phys*. **33,** L 1056.

[5] Larson, M.C., Kondow, M., Kitatani T., Yazawa Y. and Okai M.. (1997). *Electron. Lett.* **33**, 959.

[6] Hou, H.Q., Reinhardt, K.C., Kurtz, S.R., Gee, J.M., Chang, P.C. and Hammons, B.E. (1998). *Proc. 56th Int. Device Research Conference (Charlottesville,VA)* vol III B-6.

[7] Chang, P.C., Baca, A.G., Li, N. Y., Xie, X.M., Hou, H.Q. and Armour, E. (2000). *Appl. Phys. Lett*. **76** 2262.

[8] Baillargeon, J.N., Cheng, K.Y., Hofler, G.E., Pearch, P.J. and Heigh, C. (1992). *Appl. Phys. Lett.* **60** 2540.

[9] Sato, M. and Weyers, M. (1992). 19th Int. Symp. GaAs and Related Compound Semiconductors (Karuizawa). *Inst. Phys. Conf. Ser.* vol. **129** (Institute of Physics, Ltd., Bristol and Philadelphia, 1993) p 555.

[10] Ohkawa, K., Karasawa, T. and Mitsuya, T. (1991). *J. Cryst. Growth* **111** 797.

[11] Larson, M.C., Kondow, M., Kitatani, T., Yazawa, Y. and Okai, M. (1997). *Electron. Lett.* **33,** 959.

[12] Coldren, C.W., Larson, M.C., Spruytte, S.G. and Harris, J. S. (2000). *Electron. Lett.* **36**, 951.

[13] Heroux, J. B., Yang, X. and Wang, W.I. (1999). *Appl. Phys. Lett*. **75,** 2716.

[14] Kurtz, S.R., Allerman, A.A., Jones, E.D., Gee, J.M., Banas, J.J. and. Hammons, B.E. (1999). *Ibid.* **74,** 729.

[15] Xin, H.P., Tu, C.W. and Geva, M. (1999). *Ibid.* **75,** 1416.

[16] Neugebauer, J. and Van de Walle, C.G. (1995). *Phys. Rev.* B **51,** 568.

[17] Foxon, C.T., Cheng, T.S., Novikov, S.V., Lacklison, D.E., Jenkkins, L.C. Johnston, D. Orton, J.W., Hooper, S.E. Baba-Ali, N., Tansley, T.L. and Tret'yakov, V.V. (1995). *J. Cryst. Growth* **150,** 892.

[18] Bi, W.G. and Tu, C.W. (1997). Appl. Phys. Lett. **70,** 1608.

[19] Potter, R.J., Balkan, N., Adams, M.J., Chalker, P.R., Joyce, T.B. and Bullough, T.J. (2000). *Peoc. SPIE Pts.* **1 and 2, 3944** 900 (SPIE-Int. Society Optical Engineering, ISBN: 0-8194-3561-9)

[20] Sopanen, M., Xin, H.P. and Tu, C.W. (2000) *Phys. Lett*. **76,** 994.

[21] Anan, T., Nishi, K., Sugou, S. (1992). *Appl. Phys. Lett.* **60,** 25.

[22] Sánchez, J.J., Tijero, J.M.G., Hernando, J., Sánchez -Rojas, J.L., Izpura, I. (1999). *Microelectron. J*. **30,** 363.

[23] Miguel- Sánchez, J., Hopkinson, M., Gutiérrez, M., Navaretti, P. Liu, H.Y., Guzmán, A., Ulloa, J.M., Hierro, A., Muñoz, E. (2004). *J. Crystal Growth* **270,** 62.

[24] Matthews, J.W. and Blakeslee, A.E. (1974). *J. Cryst. Growth.* **27**, 118.

[25] Anderson, T.J., Chen, G., Kulakovskii, V.D., Udin, A. and Valin, J.T. (1987). *Appl. Pyhs. Lett.* **51**, 752.

[26] O'Reilly, E.P. (1989). *Semiconductor Sci. Tech*. **4**, 121

[27] Ellmers, C., Hofmann, M., Rühle, W.W., Girndt, A., Jahnke, F., Chow, W.W., Knorr, A., Koch, S.W., Hanke, C., Korte, L. and Hoyler, C. (1998). *Phys. Status Solidi* **B 206**, 407.

[28] Oduncuo lu, M. Ph. D Thesis, (2004). "A Theoretical Analysis of GaInNAs/GaAs Quantum Wells for Long Wavelength Emission", University of Gaziantep,

[29] Vurgaftman, I. and Meyer, J.R. (2003). *J. Appl. Phys.*, Vol. **94**, No. 6, 15, 3681.

[30] Hetterich, M., Grau, A., Yu Egorov, A. and Rieshert, H. (2004). *J. Phys* **16** S3151 S3159.

[31] Suemune, K. Uesugi and Walukiewicz, W. (2000). *Appl. Phys. Lett*. **77**, 3021

[32] Gönül, B. Ph. D. Thesis, (1995). "A Theoretical Study of the Threshold Current of Quantum Well Lasers", University of Surrey,

[33] Skierbiszewski, C., Perlin, P., Wisniewski, P., Knap, W., Suski, T., Walukiewicz, W., Shan, W., Yu, K.M., Ager, J.W., Haller, E.E., Geisz, J.F., Olson, J.M. (2000). *Appl. Phys. Lett*. **76**, 2409.

[34] Shan, W., Walukiewicz, W., Ager, J.W., Haller, E.E., Geisz, J.F., Friedman, D.J., Olson, J.M., Kurtz, S.R. (1999). *Phys. Rev. Lett*. **82**, 1221.

[35] Shan W, Walukiewicz W and Ager J W III, Haller E E, Geisz J F, Friedman D J, Olson J M and Kurtz S R J. (1999). *Appl. Phys.* **86**, 2349

[36] Walukiewicz, W., Shan, W., Yu, Y.M., Ager III, J.W., Haller, E.E., Miotkowski, I., Seong, M.J., Alawadiii, H. and Ramdes, A.K. (2000). *Phys. Rev. Lett.* **5**, 1552.

[37] Perlin, P., Wisniewski, P., Skierbiszewski, C., Suski, T., Kaminska, E., Subramanya, S.G., Weber, E.R., Mars, D.E. and Walukiewicz, W. (2000). *Appl. Phys. Lett*. **76**, 1279 -46.

[38] Hader, J., Koch, S.W., Moloney, J.V. and OReilly, E.P. (2000). *Appl. Phys. Lett*. **76**, 3685.

[39] Skierbiszewski, C. et al, (1999). *Physica Status Solidi* **B 216**, 135.

[40] Uesugi, K., Suemune, I., Hasegawa, T. and Akutagawa, T. (2000). *Appl. Phys. Lett*. **76**, 1285.

[41] Lindsay, A. and O'Reilly, E.P. (1999). *Solid State Commun*. **112**, 443.

[42] Hader, J., Koch, S.W., Moleney, J.V., O'Reilly, E.P. (2000). *Appl. Phys. Lett*. **77**, 630.

[43] Anan, T., Nishi, K. and Sugou, S. (1992). *Appl. Phys. Lett*., **60,** 3159.

[44] Matthews, J.W. and Blakeslee, A.E. (1974). *J. Cryst. Growth*, **27,** 118.

[45] Zory, P.S. (1993). "Quantum-Well Lasers", Academic Press, US.

[46] Vurgaftman, I. and Meyer, J.R. (2001). J. Appl. Phys., Vol. **89**, No. 11 , 14, 5815.

[47] Oduncuo lu, M. Ph.Master Thesis, (2000). "Effects of Growth Orientation on the Properties of 0 Strained Semiconductor Quantum Well Lasers"University of Gaziantep.

[48] Lawaetz, P. (1971). *Phys. Rev*. **B, 4**, 3460.

[49] Hayakawa, T., Takahashi, K., Suyama, T., Kondo, M., Yamamota, S. and Hijikata, T. (1988). *Jpn. J. Appl. Phys*. **27**, L300.

[50] Molenkamp, L.W., Eppenga, R., Thooft, G.W., Dawson, P., Foxon, C.T. and Moore, J. (1988). *Phys. Rev*. **B 38**, 4314.

[51] People, R. and Sputz, S.K. (1990). *Phys. Rev*. **B, 41**, 8431.

[52] Duggan, G., Moore, K.J., Raukema, A., Th. Jaarshma, G. and Woodbridge, K. (1992). *Phys. Rev.* **B, 45**, 4494.

[53] Osbourn, G.C. (1982). *J. Appl. Phys*. **53**, 1586.

[54] Hinckley, J.M. and Singh, J. (1990). *Phys. Rev.* **B, 42**, 3546.

[55] Pikus, G.E. and Bir, G.L. (1974). "Symmetry and Strain-induced Effects in Semiconductors", Chichester:Wiley.

[56] Caridi, E.A. and Stark, J.B. (1992). *Appl. Phys. Lett*. **60**, 1441.

[57] Hayakawa, T., Kondo, M., Suyama, T., Takahashi, K., Yamamota, S. and Hijikata, T. (1987). *Jpn. J. Appl. Phys.* **26**, L302.

[58] Hayakawa, T., Suyama, T., Takahashi, K., Kondo, M., Yamamoto, S. and Hijikata, T. (1988). *Appl. Phys. Lett*. **52**, 399.

[59] Ghiti, A., Batty, W. and O'Reilly, E.P. (1990). *Superlattices and Microstructures.* **7**, 353.

[60] Tao, I.W. (1992). *Electronics Lett.* **28**, 705.

[61] Ishihara, A. and Watanabe, H. (1994). *Jpn. J. Appl. Phys*. **33**, 1361.

[62] Smith, D.L. and Mailhot, C. (1987). Solid State Commun. 57, 919, 1986, *Phys. Rev. Lett.* **58**, 1264.

[63] Caridi, E.A., Chang, T.Y., Goossen, K.W. and Eastman, L.F. (1990). *Appl. Phys. Lett.* **56**, 659.

[64] Goossen, K.W., Caridi, E.A., Chang, T.Y., Stark, J.B., Miller, D.A.B. and Morgan, R.A. (1990). *Appl. Phys. Lett.* **56**, 715.

[65] Moise, T.S., Guido, L.J., Barker, R.C., White, J.O. and Kost, A.R. (1992). *Appl. Phys. Lett.* **60**, 2637.

[66] Sun, D. and Towe, E. (1994). *IEEE J. Quantum Electron*. **30**, 466.

[67] Kondow, M., Uomi, K., Niva, A., Kitatani, T., Watahiki, S., Yazawa, Y. (1996). *Jpn. J. Appl. Phys*. **35,** 1273.

[68] Hybertsen, M.S. (1991). *Appl. Phys. Lett*. **58**, 1759

[69] Kazarinov, R.F. and Pinto, H.R. (1994). *IEEE J. Quantum Electron*. **30**, 49

[70] Phillips, A.F., Sweeney, S.J., Adams, A.R.and Thijs, P.J.A. (1999). *IEEE J.Sel. Hijikata, Jpn. J. Top. Quantum Electronics* **5**, 401.

[71] Seki, S., Ohashi, H., Sugiura, H., Hirono, T. and Yokoyama, K. (1996). *IEEE J. Quantum Electron.* **32**,1478.

[72] Chen, T.R., Chang, B., Chiu, L.C., Yu, K.L., Margalit, S. and Yariv, A. (1983). *Appl.. Phys. Lett*. **43**, 217

[73] Kazarinov, R.F. and Belenky, G.L. (1995). *IEEE J. Quantum Electron*. **31**, 423

[74] Pan, J.W. and Chyi, J.I. (1996). *IEEE J. Quantum Electron*. **32**, 2133.

[75] Höhnsdorf, F., Koch, J., Leu, S., Stolz, W., Borchert, B., Druminski, M. (1999). *Electron. Lett*. **35,** 571.

[76] Sato, S., Satoh, S. (1999). *Electron. Lett.* **35.** 1251.

[77] Oduncuo lu, M., Gönül, B. (2005). *Physica E.* **27,** 253-261.

[78] Sato, S. and Satoh, S. (1999). *Electron. Lett.* **35**, 1251

[79] Buyanowa, I.A., Chen, W.M. and Monemar, B. (2001). *MRS Internet J. Nitride Semicond. Res.* **6**, 2.

[80] Gönül, B. and Oduncuo lu, M. (2004). *Semicond. Sci. Technol*. **19**, 23.